Enhanced Optical-OFDM With Index and Dual-Mode Modulation for Optical Wireless Systems

ALI WAQAR AZIM[ID][1]**, YANNIS LE GUENNEC**[ID][2]**, MARWA CHAFII**[ID][3]**, AND LAURENT ROS**[2]

[1]Independent Researcher
[2]Université Grenoble Alpes, CNRS, Institute of Engineering, Grenoble INP, GIPSA-LAB, 38000 Grenoble, France
[3]ETIS, UMR 8051, CY Cergy Paris Université, ENSEA, CNRS, 95000 Cergy, France

Corresponding author: Ali Waqar Azim (aliwaqarazim@gmail.com)

ABSTRACT In this article, we introduce intensity modulation and direct detection compatible enhanced optical-orthogonal frequency division multiplexing with index modulation (EO-OFDM-IM) schemes. These approaches augment the spectral efficiency (SE) relative to classical counterparts by enlarging the index domain information using the so-called virtual sub-carriers. The classical O-OFDM-IM schemes do not necessarily enhance the SE because of low cardinality of IM complex-valued sub-carrier set which is limited by constraints like Hermitian symmetry. The index domain extension for EO-OFDM-IM schemes is achieved by replacing the complex-valued sub-carriers (as in O-OFDM-IM) by twice real-valued virtual sub-carriers. The realization of non-negative signals is based on precepts of classical O-OFDM approaches, that are direct current (DC) O-OFDM and asymmetrically clipped (AC) O-OFDM. Thus, we refer to the EO-OFDM-IM approaches as DCEO-OFDM-IM and ACEO-OFDM-IM. We shall establish that in addition to improving SE, EO-OFDM-IM schemes provide extended granularity effectuating better SE/energy efficiency (EE) trade-off and improved bit error rate performance over classical counterparts. The EO-OFDM-IM schemes, however, are suitable for lower alphabet cardinalities of pulse-amplitude modulation making it difficult to attain high spectral efficiencies while maintaining EE. To circumvent this limitation, dual-mode (DM) counterparts, DCEO-OFDM-DM and ACEO-OFDM-DM are proposed. The numerical simulations shall demonstrate that the EO-OFDM-DM approaches are more energy and spectral efficient than classical O-OFDM-DM schemes and provide an advantageous granularity for EE/SE trade-off. Additionally, we use efficient index mapping and de-mapping algorithms based on Pascal's triangle, which allows investigating these approaches for peak SE by precluding the so-called sub-block partitioning. For peak SE, the use of optimal maximum-likelihood (ML) detector is cumbersome, therefore, we introduce two sub-optimal low-complexity detectors based on energy detection and ML criterion.

INDEX TERMS Optical-orthogonal frequency-division multiplexing, index modulation, intensity modulation and direct detection, optical wireless systems.

I. INTRODUCTION

Classical optical-orthogonal frequency-division multiplexing (O-OFDM) schemes for intensity-modulation and direct detection (ItM-DD), such as direct-current (DC) O-OFDM (DCO-OFDM) and asymmetrically clipped (AC) O-OFDM (ACO-OFDM) have been scrupulously studied in the literature [1], [2]. These approaches possess different spectral efficiency (SE) and energy efficiency (EE) attributes, and

their uniqueness lies in the way of how a non-negative signal is achieved. Generally, O-OFDM approaches use complex exponential orthogonal basis function, thus, at least half of the complex-valued sub-carriers are sacrificed to enforce Hermitian symmetry (HS) which is necessary to attain real-valued time-domain signal. To be more explicit, for O-OFDM with $\mathcal{N}$ complex-valued sub-carriers, only $\dot{\Omega}$ sub-carriers carry unique information, where $\dot{\Omega}$ is equal to $\mathcal{N}/2 - 1$ and $\mathcal{N}/4$, respectively for DCO-OFDM and ACO-OFDM. This establishes that considerable superfluous data has to be consolidated along with the useful

information to attain a real-valued signal. Additionally, O-OFDM schemes are ineffective of affording granularity for different spectral and energy efficiencies as their spectral efficiencies are conditional on the modulation alphabet cardinality. For example, considering base-band bandwidth [3], $\dot{\Omega}$ sub-carriers having useful information and alphabets $\dot{\mathcal{M}}$ of cardinality $\dot{M}$, the spectral efficiencies of DCO-OFDM and ACO-OFDM in bits/s/Hz are $2\dot{\Omega}\log_2(\dot{M})/\mathcal{N}$ and $\dot{\Omega}\log_2(\dot{M})/\mathcal{N}$, respectively. The EE/SE trade-off could be of vital significance when optical wireless systems (OWS) are used for Internet-of-things (IoT) and various applications which may require varying spectral efficiencies and/or energy efficiencies. Aiming to improve the SE characteristics of schemes like ACO-OFDM and unipolar-OFDM (U-OFDM) [4], hybrid O-OFDM approaches such as Layered ACO-OFDM (LACO-OFDM) and its variants [5], [6] and enhanced U-OFDM (eU-OFDM) [7] have been proposed. However, by generalizing the analysis in [3] for hybrid approaches, the peak SE attained by these approaches would be approximately half of DCO-OFDM. This is primarily due to the harmonics of non-linear clipping distortion which are substantial for these approaches.

Radio-frequency literature [8], [9] establishes that amalgamating OFDM with index modulation (IM) (i) yields a viable EE/SE trade-off by varying the number of active sub-carriers; (ii) may enhance the EE because of limited frequency resource usage; and (iii) imparts a robustness to inter-carrier interference (ICI) owing to higher sparsity of signal structure in the frequency-domain. To explore the benefits of IM for OWS, [10] and [11] explore the consolidations of IM with O-OFDM, following in DCO-OFDM-IM and ACO-OFDM-IM, where $\tilde{\kappa} \leq \tilde{\Omega}$ among $\tilde{\Omega}$ complex-valued sub-carriers are activated, where $\tilde{\Omega} = \dot{\Omega}$. However, despite the feasibility of O-OFDM-IM approaches, they have several shortcomings. First, for the same alphabet cardinality, the (peak) SE of O-OFDM-IM remains close to that of O-OFDM. This is due to reduced cardinality of set of IM complex-valued sub-carriers as HS eliminates functionality of a significant number of complex-valued sub-carriers. Thus, the index domain information is lessened as the amount of legitimate sub-carrier activation patterns (SAPs) is reduced. To be more precise, the cardinality of the set of complex-valued sub-carriers for IM in O-OFDM-IM schemes is $\tilde{\Omega}$, which results in $\dot{\mathcal{D}} = 2^{\lfloor \log_2 \binom{\tilde{\Omega}}{\tilde{\kappa}} \rfloor}$ legitimate SAPs, where $\binom{\cdot}{\cdot}$ is the binomial coefficient and $\lfloor \cdot \rfloor$ is the floor function. Generally, the index domain information embodied in the SAPs of O-OFDM-IM approaches (evaluated considering $\tilde{\Omega}$) is not substantial to offer an increase in SE over O-OFDM schemes. Second, using alphabet $\tilde{\mathcal{M}}$ of cardinality $\tilde{M}$, such that $\tilde{M} = \dot{M}$, the EE for peak SE for O-OFDM-IM over O-OFDM is realizable if and only if $\tilde{\kappa} < \tilde{\Omega}$. However, it may not always be the case with O-OFDM-IM schemes as all the complex-valued sub-carriers, i.e., $\tilde{\kappa} = \tilde{\Omega}$ may have to be activated to obtain peak SE [12]. Thus, it is dubious that any EE over O-OFDM can be attained for peak SE.

Nevertheless, aforementioned O-OFDM-IM schemes offer the prospect of EE/SE trade-off. In [12], we proposed DC optical-Fast OFDM with index modulation (DCO-FOFDM-IM) for OWS which is capable of significantly augmenting the SE compared to DCO-OFDM-IM. DCO-FOFDM-IM uses real-valued sub-carriers and pulse-amplitude modulation (PAM) alphabets rather than employing complex-valued sub-carriers and quadrature-amplitude modulation (QAM) alphabets as in DCO-OFDM-IM, thus, HS can be averted. However, the complexity of DCO-FOFDM-IM is marginally higher (than classical counterparts) as additional discrete Fourier transform (DFT) and its inverse, i.e., IDFT is required to equalize the received signal. Hereby, we shall not consider DCO-FOFDM-IM as a benchmark because our objective is to investigate approaches in O-OFDM-IM framework. It may also be noticed that when we use only one index for IM in DCO-FOFDM-IM, it corresponds to DC-frequency shift keying (DC-FSK) scheme that we developed for IoT communications in [13].

To overcome limited SE augmentation in O-OFDM-IM schemes, [11] and [14] consider dual-mode (DM) IM with DCO-OFDM, referred to as DCO-OFDM-DM. Though combining DM with ACO-OFDM has not been considered in the literature, we believe that it is straightforward, therefore, we will implement it to serve as a benchmark. Nonetheless, [14] and [11] propose a DM variant of U-OFDM, i.e., U-OFDM-DM. We foresee that the performance of ACO-OFDM-DM and U-OFDM-DM will be comparable as the literature claims that both ACO-OFDM and U-OFDM perform identically [7]. We choose to consider ACO-OFDM-DM as benchmark because U-OFDM-DM is sensitive to DC component fluctuation over the symbol duration.

In O-OFDM-DM, the useable complex-valued sub-carriers $\tilde{\Omega}$ are partitioned into two groups, that are group A and group B. The complex-valued sub-carriers in each group are modulated using two distinguishable complex-valued alphabets $\tilde{\mathcal{M}}_a$ and $\tilde{\mathcal{M}}_b$ of sizes $\tilde{M}_a$ and $\tilde{M}_b$, respectively, where $\tilde{\mathcal{M}}_a \cap \tilde{\mathcal{M}}_b = \phi$, with ϕ being an empty set. Group A transmits the index domain information by activating $\tilde{\kappa}$ complex-valued sub-carriers among $\tilde{\Omega}$ based on a given SAP, whilst, group B comprises the remaining complex-valued sub-carriers equal to $\tilde{\Omega} - \tilde{\kappa}$. The literature suggests that O-OFDM-DM schemes attains higher SE than O-OFDM/O-OFDM-IM at the cost of poorer EE [11], [14].

For O-OFDM-IM and O-OFDM-DM schemes, ideally, an optimal maximum-likelihood (ML) detector should be employed for joint detection of the SAP and the modulated alphabets. However, the complexity of the ML detector is prohibitively high. For example, for peak SE, the complexity of ML detector for O-OFDM-IM schemes is $\mathcal{O}(\tilde{\mathcal{D}}\tilde{M}^{\tilde{\kappa}}/\tilde{\Omega} + \tilde{\kappa}\tilde{M}/\tilde{\Omega})$ [15]. For O-OFDM-DM, the complexity is even loftier. To alleviate the complexity of ML detector, $\tilde{\Omega}$ are divided into cluster/sub-blocks using so-called sub-carrier partitioning (SP). Thus, the number of complex-valued sub-carriers per sub-block are $\ll \tilde{\Omega}$. The SP based transmitter

and receiver architectures have become state-of-art design to reduce the ML detector complexity [8]. Implementing the ML detector per sub-block can appreciably curtail the complexity of the receiver. Using SP, the inherent inefficiency of combinatorial mapping and de-mapping can also be counterbalanced [16]. Considering an SP-free architecture, which refers to the case when peak SE is realized, the complexity of combinatorial mapping in O-OFDM-IM schemes is $\mathcal{O}(\tilde{\Omega})$ [17]. Furthermore, [18] affirms that the implicit inefficiency of combinatorial mapping could add transmission delays, which might affect the overall SE. Thus, the SP based architectures lessen the transmission delays as it would be feasible to use look-up-table (LUT) for combinatorial mapping and de-mapping. However, SP reduces the peak SE proportionally to the number of sub-blocks [17], [18].

Against the background, we propose two enhanced O-OFDM-IM (EO-OFDM-IM) and two enhanced O-OFDM-DM (EO-OFDM-DM) approaches aiming to augment both the SE and the EE performances relative to the classical benchmarks. We epitomize the principles and advantages of the proposed approaches as follows:

- The EO-OFDM-IM schemes, namely DCEO-OFDM-IM and ACEO-OFDM-IM enhance the SE (compared to the classical benchmarks) by using the so-called virtual sub-carriers. In the proposed schemes, rather than considering $\tilde{\Omega}$ complex-valued sub-carriers as in O-OFDM-IM ($\mathcal{N}/2 - 1$ for DCO-OFDM and $\mathcal{N}/4$ for ACO-OFDM), we consider Ω real-valued virtual sub-carriers, where Ω is equal to $\mathcal{N}-2$ and $\mathcal{N}/2$ respectively, for DCEO-OFDM-IM and ACEO-OFDM-IM. This permits to double the number of indices for the index domain information. This idea is somewhat similar to what we developed for DCO-FOFDM-IM, but here we develop the schemes in O-OFDM-IM framework which permits to use the discrete Fourier transform (DFT) and its inverse, i.e., IDFT and thereby classical equalization methods without increasing the complexity. Based on the chosen SAP, $\kappa < \Omega$ virtual sub-carriers are activated which modulate real-valued alphabet, $\mathcal{M}$ of cardinality M. The amount of legitimate SAPs for EO-OFDM-IM schemes is $\mathcal{D} = 2^{\lfloor \log_2 \binom{\Omega}{\kappa} \rfloor}$. It can be discerned that $\mathcal{D} > \tilde{\mathcal{D}}$ because using Pascal's triangle (PT), we can readily verify that $\binom{\Omega}{\kappa}$ would be greater than $\binom{\tilde{\Omega}}{\tilde{\kappa}}$ when $\Omega > \tilde{\Omega}$ and $\kappa > \tilde{\kappa}$. Thus, the index domain information is enlarged, culminating in higher spectral efficiencies for EO-OFDM-IM schemes. We shall demonstrate that the EE performance of EO-OFDM-IM for low spectral efficiencies is identical to that of O-OFDM-IM, whilst for high spectral efficiencies, EO-OFDM-IM schemes are more energy-efficient. Furthermore, unlike O-OFDM, the EO-OFDM-IM provides an advantageous EE/SE trade-off. It may also be noticed that $\kappa = 1$ for DCEO-OFDM-IM with 2-PAM corresponds to DC-frequency and (binary) phase shift keying (DC-FPSK) approach that we developed in [19].

- The EO-OFDM-IM schemes are extended to develop DM variants, resulting in DCEO-OFDM-DM and ACEO-OFDM-DM approaches. Like EO-OFDM-IM, for EO-OFDM-DM, κ virtual sub-carriers among Ω are used for IM and are modulated with real-valued alphabet, $\mathcal{M}_a$ of cardinality M_a. The remaining $\Omega-\kappa$ virtual sub-carrier modulate a different real-valued alphabet $\mathcal{M}_b$ of size M_b. Essentially, the average symbol energy of the alphabets modulated onto the IM and non-IM virtual sub-carriers is different, which simplifies the detection problem at the receiver. The reason for higher achievable SE for the DM approaches is again the enlargement of index domain information. We shall demonstrate that the EO-OFDM-DM approaches can attain considerably higher spectral efficiencies than O-OFDM-DM schemes while sustaining better EE.

- For the proposed approaches, we consider SP-free architectures for transmitter and receiver, hence, all virtual sub-carriers are treated for IM. Consequently, the peak SE can be attained which is inconceivable when SP is adopted. Since the ML detector is complex and the combinatorial mapping and de-mapping is inefficient, therefore, the SP-free architectures of the transmitter and receiver are aided by the use of low-complexity detectors and efficient index mapping and de-mapping algorithms based on PT. The low-complexity detectors are based on energy detection and ML criterion.

A. NOTATIONS

We use calligraphic letter $\mathcal{N}$ for the complex-valued sub-carrier. Lowercase and uppercase boldface letters are used for discrete time-domain signal vector, e.g., $\mathbf{x}$ and frequency-domain symbol vector like $\mathbf{X}$, respectively. The exceptions are $\mathbf{F}$ and $\mathbf{H}$ which represent the DFT matrix and channel state matrix (CSM), respectively. The (k, n)th element of the DFT matrix is $[\mathbf{F}]_{k,n} = \mathcal{N}^{-1/2} \exp\left(-j2\pi kn\mathcal{N}^{-1}\right)$. The kth elements of the discrete time-domain signal $\mathbf{x}$ and frequency-domain symbol $\mathbf{X}$ are given as x_k and $X[k]$, respectively. The non-negative counterpart of discrete time-domain signal $\mathbf{x}$ is given as $(\mathbf{x})^+$. The analog intensity waveform is $x(t)$. Furthermore, as a general rule, we use the parameters (not vectors) with tilde and dot, e.g., $\tilde{\Omega}$ and $\dot{\Omega}$ for classical O-OFDM-IM and O-OFDM approaches, respectively. The diagonalization of a vector is expressed using diag$\{\cdot\}$. ψ_m is the mth harmonic number, $\binom{\cdot}{\cdot}$ is the binomial coefficient, $\log_2(\cdot)$ is logarithm to the base 2, $\log(\cdot)$ is the natural logarithm, and $\lfloor \cdot \rfloor$ is the floor function. The operator $[\cdot]^T$ denotes transpose, $[\cdot]^H$ Hermitian conjugate transpose, $[\cdot]^*$ complex conjugate, $\otimes$ convolution, $\mathbb{E}\{\cdot\}$ expectation, $\| \cdot \|^2$ Euclidean norm, $| \cdot |$ cardinality, and $\langle \cdot ; \cdot \rangle$ dot product. Moreover, $\Re\{\cdot\}$ and $\Im\{\cdot\}$ extract the real and imaginary components of a complex-valued number.

B. PAPER ORGANIZATION

The remainder of the article is organized as follows: In section II, we present the system model and the index
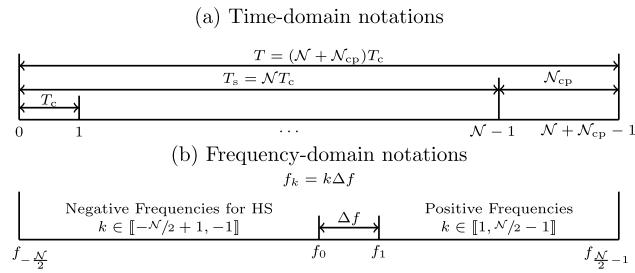
FIGURE 1. (a) Time-domain notations; and (b) frequency-domain notations.

mapping/de-mapping algorithms based on PT. Section III elucidates the transmitter and receiver architectures of EO-OFDM-IM, whereas the performances of these approaches in terms of SE, EE, bit error rate (BER) are presented in Section IV. EO-OFDM-DM approaches are presented in Section V. Section VI presents the performances of the EO-OFDM-DM schemes for above-mentioned parameters. Finally, based on the results, conclusions are rendered in Section VII.

II. PRELIMINARIES
A. SYSTEM MODEL
For clarity, we present the time-domain and frequency-domain notations used in the sequel in Fig. 1. Consider a generalized system model for EO-OFDM-IM and EO-OFDM-DM schemes, where the frequency-domain symbol $\mathbf{X} = \left[X\left[-\frac{\mathcal{N}}{2}\right], \cdots, 0, \cdots, X\left[\frac{\mathcal{N}}{2} - 1\right]\right]^{\mathrm{T}}$ comprises $\mathcal{N}$ complex-valued sub-carriers at frequencies $f_k = k\Delta f$ with indices $k \in [\![-\mathcal{N}/2, \mathcal{N}/2 - 1]\!]$, where $\Delta f = 1/T_s$ with T_s being the symbol duration. For implementation via DFT and its inverse, the frequencies at f_0 and $f_{-\mathcal{N}/2}$ are not modulated, whilst the positive frequencies with $k \in [\![1, \mathcal{N}/2 - 1]\!]$ can modulate complex-valued data. On the other hand, the negative frequencies with $k \in [\![-\mathcal{N}/2 + 1, -1]\!]$ incorporate HS, i.e., $X\left[-\frac{\mathcal{N}}{2} + k\right] = X^*[k]$ for $k \in [\![1, \mathcal{N}/2 - 1]\!]$. This indicates that only $\mathcal{N}/2 - 1$ complex-valued sub-carriers at frequencies $k \in [\![1, \mathcal{N}/2 - 1]\!]$ are available for IM. It is highlighted that unlike O-OFDM-IM/O-OFDM-DM schemes, in EO-OFDM-IM/EO-OFDM-DM, $\mathbf{X}$ is attained considering the in-phase and quadrature components of $\tilde{\Omega}$ complex-valued sub-carriers separately for IM. The details of which shall be presented in detail in the subsequent sections.

The time-domain counterpart of $\mathbf{X}$, i.e., $\mathbf{x}$ is attained after IDFT of $\mathbf{X}$ as

$$\mathbf{x} = [x_0, x_1, \cdots, x_{\mathcal{N}-1}]^{\mathrm{T}} = \mathbf{F}^{\mathrm{H}}\mathbf{X}. \qquad (1)$$

A cyclic prefix (CP) of length $\mathcal{N}_{\mathrm{cp}}$ is appended to $\mathbf{x}$. The extended symbol duration of the time-domain signal is $T = \left(\mathcal{N} + \mathcal{N}_{\mathrm{cp}}\right)T_c = T_s + T_{\mathrm{cp}}$, where T_c is the chip (i.e., sample) duration. $\mathbf{x}$ is bipolar, accordingly, time-domain processing is required to make the signal non-negative expressed as $(\mathbf{x})^+$ for transmission via light-emitting diodes (LEDs) using

ItM-DD. After digital-to-analog conversion, the electrical intensity waveform, $x(t) \geq 0$ is applied to the LED assumed to be operating within the linear region. $x(t)$ is transformed to an optical intensity waveform, $s(t) = \rho x(t)$, where ρ (Watt/Ampere) is the electrical-to-optical conversion factor. $s(t)$ is then transmitted to optical wireless channel having impulse response $h(t)$. The discrete-time impulse response coefficients vector is $\mathbf{h} = \left[h_0, h_1, \cdots, h_{\mathcal{N}-1}\right]^{\mathrm{T}}$. Considering a P-tap discrete channel, the first $P \leq \mathcal{N}$ coefficients of $\mathbf{h}$ are non zero. The length of affixed CP is $\mathcal{N}_{\mathrm{cp}} \geq P$. The photo-detected waveform is $u(t) = \varepsilon\left(h(t) \otimes s(t)\right)$, where ε (Ampere/Watt) is the responsitivity of the photo-diode (PD). PD is considered being operating within the linear range. Without loss of generality, we consider $\rho = \varepsilon = 1$ as customarily assumed in the literature [2], [3], [12], [13]. The photo-detected waveform is contaminated by the ambient noise resulting in $y(t)$ which is given as $y(t) = h(t) \otimes x(t) + n(t)$, where $n(t)$ is additive white Gaussian noise with mono-lateral power spectral density of N_0. After analog-to-digital conversion and removal of CP, the time series representation of the received signal is given as

$$\mathbf{y} = [y_0, y_1, \cdots, y_{\mathcal{N}-1}]^{\mathrm{T}} = \mathbf{H}(\mathbf{x})^+ + \mathbf{n}, \qquad (2)$$

where $\mathbf{H} = \mathrm{diag}\left\{h_0, h_1, \cdots, h_{\mathcal{N}-1}\right\}$ is the CSM of size $\mathcal{N} \times \mathcal{N}$ and $\mathbf{n} = \left[n_0, n_1, \cdots, n_{\mathcal{N}-1}\right]^{\mathrm{T}}$ is white real-valued Gaussian noise vector. The CSM matrix is diagonalized as

$$\mathbf{H} = \mathbf{F}^{\mathrm{H}}\Lambda\mathbf{F}, \qquad (3)$$

where Λ is $\mathcal{N} \times \mathcal{N}$ diagonal matrix of eigenvalues $\Lambda = \left[\Lambda_0, \Lambda_1, \cdots, \Lambda_{\mathcal{N}-1}\right]^{\mathrm{T}}$ of $\mathbf{H}$.

Afterwards, by applying DFT on $\mathbf{y}$, the frequency domain symbol $\mathbf{Y} = \left[Y\left[-\frac{\mathcal{N}}{2}\right], \cdots, 0, \cdots, Y\left[\frac{\mathcal{N}}{2} - 1\right]\right]^{\mathrm{T}}$ is attained as

$$\mathbf{Y} = \mathbf{F}\mathbf{y} = \mathbf{F}\mathbf{F}^{\mathrm{H}}\Lambda\mathbf{F}(\mathbf{x})^+ + \mathbf{F}\mathbf{n} = \Lambda\mathbf{X} + \mathbf{N}, \qquad (4)$$

where $\mathbf{N} = \left[N\left[-\frac{\mathcal{N}}{2}\right], \cdots, 0, \cdots, N\left[\frac{\mathcal{N}}{2} - 1\right]\right]^{\mathrm{T}}$ is the frequency-domain Gaussian noise vector. A zero-forcing (ZF) equalizer given as

$$\mathbf{W}_{\mathrm{ZF}} = \Lambda^{-1}, \qquad (5)$$

is used for frequency-domain equalization of $\mathbf{Y}$, resulting in

$$\hat{\mathbf{Y}} = \mathbf{W}_{\mathrm{ZF}}\mathbf{Y} = \hat{\mathbf{X}} + \mathbf{Z}, \qquad (6)$$

where $\hat{\mathbf{Y}} = \left[\hat{Y}\left[-\frac{\mathcal{N}}{2}\right], \cdots, 0, \cdots, \hat{Y}\left[\frac{\mathcal{N}}{2} - 1\right]\right]^{\mathrm{T}}$, $\hat{\mathbf{X}} = \left[\hat{X}\left[-\frac{\mathcal{N}}{2}\right], \cdots, 0, \cdots, \hat{X}\left[\frac{\mathcal{N}}{2} - 1\right]\right]^{\mathrm{T}}$ is the received counterpart of the complex-valued frequency-domain signal $\mathbf{X}$, and $\mathbf{Z} = \mathbf{W}_{\mathrm{ZF}}^{-1}\mathbf{N} = \left[Z\left[-\frac{\mathcal{N}}{2}\right], \cdots, 0, \cdots, Z\left[\frac{\mathcal{N}}{2} - 1\right]\right]^{\mathrm{T}}$ is the frequency-domain colored noise vector.

In case of line-of-sight (LOS) channel, the CSM consists of LOS channel coefficient h_0 on its diagonal. Therefore, (2) can be simplified as $\hat{\mathbf{y}} = h_0^{-1}\mathbf{y}$, which results in $\hat{\mathbf{Y}}$ after the DFT.

The virtual sub-carriers from which the transmitted information can be extracted are attained using $\hat{\mathbf{Y}}$. The details are provided in the subsequent sections.

B. INDEX MAPPING AND DE-MAPPING

For clarity, in this section, we shall adopt the term *sub-carriers* for both complex-valued sub-carriers and virtual sub-carriers. Consider a generalized scenario where Ω sub-carriers are available for IM, among which, κ are to be activated conforming to the chosen SAP, $\boldsymbol{\theta} = \{\theta_1, \theta_2, \cdots, \theta_\kappa\}$, whereby the indices are arranged in descending order as $\theta_1 > \theta_2 > \cdots > \theta_\kappa \geq 0$. $\boldsymbol{\theta}$ is determined via index mapping algorithm and singles out the sub-carriers to be activated from the set $\boldsymbol{\Theta} = \{0, 1, \cdots, \Omega - 1\}$. Reference [16] proposes an index mapping algorithm known as combinatorial mapping which is commonly used in state-of-the-art IM/DM schemes [9]. In combinatorial mapping, $\binom{\Omega}{\kappa}$ SAPs are generated and listed in lexicographical order, among which, the first 2^λ SAPs are adopted to construct a bijective mapping relation to $V = 2^\lambda$ integers, where $\lambda = \lfloor \log_2 \binom{\Omega}{\kappa} \rfloor$ is the number of bits to be encoded for IM. Thus, any integer between the range $V \in [0, 2^\lambda - 1]$ have a unique representation in a strictly decreasing sequence $\boldsymbol{\theta}$ of length κ. The relationship between V and $\boldsymbol{\theta}$ is given as

$$V = \sum_{i=1}^{\kappa} \binom{\theta_{\kappa-i+1}}{\kappa - i + 1}. \tag{7}$$

Combinatorial mapping is required at the transmitter to determine $\boldsymbol{\theta}$, while a reverse operation, i.e., combinatorial de-mapping (via index de-mapping) is performed at the receiver to identify the integer corresponding to the SAP. The complexity of combinatorial mapping for peak SE is $\mathcal{O}(\Omega^2)$ [17], therefore, SP is unavoidable to reduce the overall complexity of the system [17]. Furthermore, [17] suggests that transmission delays owing to inefficiency of combinatorial mapping may manifest as a reduction in overall SE. This indicates that combinatorial mapping and de-mapping may not be the best option for index mapping and de-mapping, respectively.

Assuming that the maximum number of sub-carriers to be activated is $\kappa \leq \Omega/2$, [17] proposes linear mapping and de-mapping algorithms having complexity of $\mathcal{O}(\Omega)$, which is considerably less than that of combinatorial mapping and de-mapping. Like combinatorial mapping, these algorithms maps/de-maps the integers between the range $V \in [0, 2^\lambda - 1]$ to an exclusive $\boldsymbol{\theta}$ of length κ or vice versa. The outputs of both the combinatorial mapping and the linear mapping are identical. By leveraging the benefits of the linear mapping and de-mapping algorithms, [17] recommends the use of SP-free transmitter and receiver architectures. Nevertheless, the underlying presumption of $\kappa \leq \Omega/2$ is not consistently valid to attain the peak SE. To be more precise, if we only consider IM bits, the above-mentioned condition is true to attain maximum index domain information. However, when IM bits and constellation bits are examined in tandem

---

Algorithm 1 PT Based Index Mapping Algorithm

Input: Pascal's Triangle, $\mathcal{P}(\Omega, \kappa)$, Ω, κ, V
Output: $\boldsymbol{\theta} = \{\theta_1, \theta_2, \cdots, \theta_\kappa\}$, such that $\theta_1 > \theta_2 > \cdots > \theta_\kappa \geq 0$
    Initialization: $l = [\![1, \Omega]\!]$, $\dot{\boldsymbol{\theta}} \leftarrow$ empty vector
1: **for** $i = 1$ to κ **do**
2:    **if** $V \neq 0$ **then**
3:      $\dot{\theta}_i \rightarrow$ maximum l satisfying $\mathcal{P}(l, \kappa - i + 1) \leq V$
4:    **end if**
5:    **if** $V = 0$ **then**
6:      $\dot{\theta}_i \rightarrow$ maximum l satisfying $\mathcal{P}(l, \kappa - i + 1) = 0$
7:    **end if**
8:    $V = V - \mathcal{P}(\dot{\theta}_i, \kappa - i + 1)$
9:    $l = [\![1, \dot{\theta}_i - 1]\!]$
10: **end for**
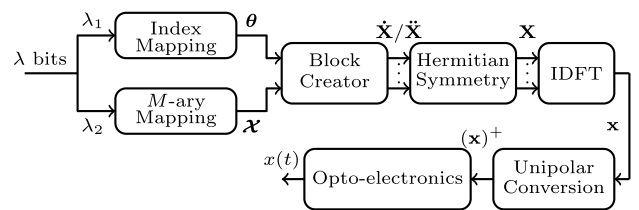11: **return** $\boldsymbol{\theta} = \dot{\boldsymbol{\theta}} - 1$

FIGURE 2. Generalized transmitter architecture for EO-OFDM-IM schemes.

to attain the peak SE, then, the condition, $\kappa \leq \Omega/2$ is not valid anymore. For example, [12] establishes that for DCO-OFDM-IM with $\Omega = 15$ and employing 4 QAM, the number of complex-valued sub-carriers to attain peak SE are $\kappa = 11$ signifying a divergence from the condition $\kappa \leq \Omega/2$. Consequently, owing to the limitation of the linear mapping and de-mapping algorithms, if $\kappa > \Omega/2$, these algorithms will not work.

In [20], the authors suggest that $\boldsymbol{\theta}$ can be attained using queries of the binomial coefficient $\binom{\theta_{\kappa-i+1}}{\kappa-i+1}$ as in (7) from PT of dimensions $\Omega \times \kappa$. As PT consists of the binomial coefficients $\binom{\theta_{\kappa-i+1}}{\kappa-i+1}$ corresponding to all Ω and κ, henceforth, there is no need to evaluate them from scratch; which considerably reduces the complexity of the index mapping and de-mapping. The complexity of PT based index mapping and de-mapping algorithms is $\mathcal{O}(\Omega)$ [20] and requires a LUT of dimensions $\Omega \times \kappa$ to be buffered. However, the limiting condition for linear mapping and de-mapping, i.e., $\kappa \leq \Omega/2$ is not an issue for PT based approaches which makes them more effective. Appreciating the notion of adopting PT for index mapping and de-mapping in [20], we provide algorithms to do so (cf. Alg. 1 and Alg. 2) which were not provided in [20]. It is affirmed that the outputs of PT based index mapping and de-mapping algorithms are the same as that of combinatorial mapping and de-mapping, respectively. In the sequel, we adopt PT based mapping and de-mapping for our proposed schemes as we employ SP-free architectures for the transmitter and the receiver.

Algorithm 2 PT Based Index De-Mapping Algorithm

Input: Pascal's Triangle, $\mathcal{P}(\Omega, \kappa)$, κ, $\boldsymbol{\theta} = \theta_1, \theta_2, \cdots, \theta_\kappa$
    such that $\theta_1 > \theta_2 > \cdots > \theta_\kappa \geq 0$
Output: V
    Initialization : $V = 0, Z = 0, \dot{\boldsymbol{\theta}} = \boldsymbol{\theta} + 1$
1: **for** $i = 1$ to κ **do**
2:    $Z = \mathcal{P}(\dot{\theta}, \kappa - i + 1)$
3:    $V = V + Z$
4: **end for**
5: **return** V

III. PROPOSED ENHANCED O-OFDM INDEX MODULATION SCHEMES

In this section, we present the transceiver structure of proposed EO-OFDM-IM in detail. First, we present the transmitter architecture and subsequently, the low-complexity detectors are presented.

A. TRANSMITTER ARCHITECTURE

A generalized transmitter for EO-OFDM-IM is presented in Fig. 2. In EO-OFDM-IM schemes, rather than considering $\tilde{\Omega}$ complex-valued sub-carriers for IM, we consider $\Omega = 2\tilde{\Omega}$ real-valued virtual sub-carriers. The underlying idea is to consider the in-phase and quadrature phase components of the $\tilde{\Omega}$ complex-valued sub-carriers separately and use real-valued PAM alphabets. We recall that the total number of virtual sub-carriers available for IM in DCEO-OFDM-IM and ACEO-OFDM-IM are respectively equal to $\mathcal{N} - 2$ and $\mathcal{N}/2$.

The equiprobable bit sequence of length λ is split into IM bits, λ_1, and the constellation bits, λ_2. λ_1 is equal to

$$\lambda_1 = \left\lfloor \log_2 \binom{\Omega}{\kappa} \right\rfloor. \tag{8}$$

Using λ_1, an integer $V \in [0, 2^{\lambda_1} - 1]$ is generated which is adopted to determine $\boldsymbol{\theta} = \{\theta_1, \theta_2, \cdots, \theta_\kappa\} \in \boldsymbol{\Theta}$ using PT index mapping algorithm (cf. Alg. 1). $\boldsymbol{\Theta} = \{0, 1, \cdots, \Omega - 1\}$ is the set of virtual sub-carriers for IM having cardinality $|\boldsymbol{\Theta}| = \Omega$.

λ_2 bits are utilized to generate κ real-valued symbols, $\mathcal{X} = [\mathcal{X}[0], \mathcal{X}[1], \cdots, \mathcal{X}[\kappa - 1]]^{\mathrm{T}} \in \mathcal{M}$ to be modulated onto the virtual sub-carriers identified via $\boldsymbol{\theta}$, where $\mathcal{M}$ represents the PAM alphabet of cardinality M. Accordingly, λ_2 bits are equal to

$$\lambda_2 = \log_2(M^\kappa). \tag{9}$$

The total number of bits, λ transmitted per EO-OFDM-IM symbol of duration T_{s}[1] is obtained summing (8) and (9), which is equal to

$$\lambda = \left\lfloor \log_2 \binom{\Omega}{\kappa} \right\rfloor + \log_2(M^\kappa). \tag{10}$$

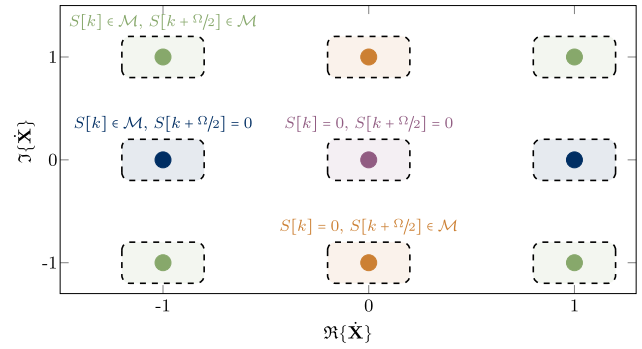[1]For simplicity we do not consider the extended symbol duration T after CP annexation.

FIGURE 3. Signal space for EO-OFDM-IM for $\mathcal{M} \in \{-1, 1\}$, i.e., 2-PAM alphabets and $k \in [\![0, \Omega/2 - 1]\!]$.

Using $\boldsymbol{\theta}$ and $\mathcal{X}$, the vector $\mathbf{S} = [S[0], S[1], \cdots, S[\Omega-1]]^{\mathrm{T}}$ comprising Ω real-valued virtual sub-carriers is obtained as

$$S[k] = \begin{cases} \mathcal{X}[k], & k \in \boldsymbol{\theta} \\ 0, & \text{otherwise} \end{cases}, \quad k \in [\![0, \Omega - 1]\!]. \tag{11}$$

Subsequently, $\mathbf{S}$ is split into two sub-vectors; which are combined to attain $\dot{\mathbf{X}} = [\dot{X}[0], \dot{X}[1], \cdots, \dot{X}[\Omega/2 - 1]]^{\mathrm{T}}$, whose kth element is given as:

$$\dot{X}[k] = S[k] + jS\left[k + \frac{\Omega}{2}\right], \tag{12}$$

where $j^2 = -1$ and $k \in [\![0, \Omega/2 - 1]\!]$. It may be noticed that first $\Omega/2$ elements (virtual sub-carriers) of $\mathbf{S}$ are the in-phase components, while the last $\Omega/2$ components are the quadrature components of $\dot{\mathbf{X}}$. Based on $\boldsymbol{\theta}$, the elements of vector $\dot{\mathbf{X}}$ can be null, real-valued or complex-valued. The signal space of $\dot{\mathbf{X}}$ using 2-PAM is presented in Fig. 3 from which we observe that there are 9 distinct points in the signal space. This indicates that for the classical O-OFDM or O-OFDM-IM schemes, the alphabets with higher cardinalities may be needed to match the peak spectral efficiencies of EO-OFDM-IM approaches.

For DCEO-OFDM-IM, the frequency-domain signal $\mathbf{X}$ having $\mathcal{N}/2 - 1$ useful complex-valued sub-carriers is forthrightly obtained by imposing HS as $\mathbf{X} = [0, \dot{\mathbf{X}}*, 0, \dot{\mathbf{X}}]$. On the other hand, for ACEO-OFDM-IM, first $\dot{\mathbf{X}}$ is interleaved with zeros as $\ddot{\mathbf{X}} = [\dot{X}[0], 0, \dot{X}[1], 0, \cdots, \dot{X}[\frac{\Omega}{2} - 1]]^{\mathrm{T}}$ which is followed by imposition of HS as $\mathbf{X} = [0, \ddot{\mathbf{X}}*, 0, \ddot{\mathbf{X}}]$. It may be noticed that only odd sub-carriers in $\mathbf{X}$ for ACEO-OFDM-IM can have any point from the signal space.

$\mathbf{X}$ is treated using DFT matrix, $\mathbf{F}$ of size $\mathcal{N} \times \mathcal{N}$ to obtain a real-valued time-domain signal $\mathbf{x}$ comprising $\mathcal{N}$ chips. The average electrical symbol energy and average symbol power of $\mathbf{x}$ is $\mathbb{E}\{\|x_k\|^2\} = \mathbb{E}\{\sum_{k=0}^{\mathcal{N}-1} x_k^2\} = 2\kappa E_{\mathrm{avg}}$ and $\sigma_x^2 = \mathbb{E}\{\|x_k\|^2\}/\mathcal{N}$, respectively. E_{avg} is the average M-ary PAM symbol energy equal to $(M^2 - 1)/3$. $\mathbf{x}$ is bipolar, thus, some time-domain processing is imperative to attain a non-negative real-valued time-domain signal consistent with ItM-DD. For DCEO-OFDM-IM, a bias equal to $\beta = \mu\sigma_x$ is added which is followed by a zero level clipping of negative amplitude
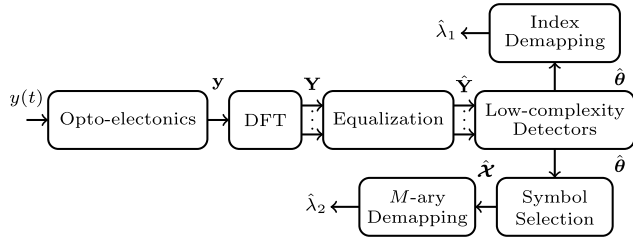
FIGURE 4. Generalized receiver architecture for EO-OFDM-IM schemes.

excursions to attain $(\mathbf{x})^+$, where μ is a constant. The bias on a decibel (dB) scale is $10 \log_{10}(\mu^2 + 1)$. For ACEO-OFDM-IM, $\mathbf{x}$ features an anti-symmetric property, i.e., $x_k = -x_{k+\mathcal{N}/2}$ for $k \in \llbracket 0, \Omega/2 - 1 \rrbracket$. Owing to this anti-symmetric property, the negative excursions of $\mathbf{x}$ are clipped to obtain a non-negative time-domain signal, $(\mathbf{x})^+$. Subsequently, after CP addition and opto-electronic processing, the analog electrical intensity waveform, $x(t)$ is transmitted to the optical wireless channel using an LED.

For DCEO-OFDM-IM and ACEO-OFDM-IM, the average electrical symbol energy of $(\mathbf{x})^+$ is $\mathbb{E}\left\{\|x_k^+\|^2\right\} = \mathbb{E}\left\{\sum_{k=0}^{\mathcal{N}-1}(x_k^+)^2\right\} = 2\kappa E_{\text{avg}} + \mathcal{N}\mu^2$ and $\mathbb{E}\left\{\|x_k^+\|^2\right\} = \kappa E_{\text{avg}}$, respectively. Whereas, the average electrical power of EO-OFDM-IM is equal to $\sigma^2 = \mathbb{E}\left\{\|x_k^+\|^2\right\}/\mathcal{N}$.

B. RECEIVER ARCHITECTURES

As aforementioned, implementing the optimal ML detector is cumbersome for SP-free architectures. As we are using SP-free architectures for the transmitter, henceforth, we present two sub-optimal low-complexity detectors, among them, one is based on energy detection, whereas, the other is based on the ML criterion. A generalized receiver architecture for EO-OFDM-IM is given in Fig. 4, where low-complexity detector are employed.

Recall that the received frequency-domain symbol is $\hat{\mathbf{Y}}$. The first step is to elicit the useful information from $\mathcal{N}/2 - 1$ complex-valued sub-carriers of the positive frequencies as

$$\hat{Y}[k] = \begin{cases} \hat{Y}[k+1], & \text{DCEO-OFDM-IM} \\ 2\hat{Y}[2k+1], & \text{ACEO-OFDM-IM,} \end{cases} \quad (13)$$

where $k \in \llbracket 0, \Omega/2 - 1 \rrbracket$. Using $\hat{\mathbf{Y}} = [\hat{Y}[0], \hat{Y}[1], \cdots, \hat{Y}[\frac{\Omega}{2} - 1]]^{\text{T}}$, the virtual sub-carriers vector $\hat{\hat{\mathbf{Y}}} = [\hat{\hat{Y}}[0], \hat{\hat{Y}}[1], \cdots, \hat{\hat{Y}}[\Omega - 1]]^{\text{T}}$ is extracted as

$$\hat{\hat{\mathbf{Y}}} = [\Re\{\hat{\mathbf{Y}}\} \quad \Im\{\hat{\mathbf{Y}}\}], \quad (14)$$

using which we determine $\hat{\boldsymbol{\theta}}$ and $\hat{\boldsymbol{\mathcal{X}}}$ modulated onto the virtual sub-carriers. The details of the operating principles of the detectors are outlined in the subsequent subsections.

1) ENERGY DETECTOR

The sub-optimal energy detectors are frequently adopted for IM approaches [12], [21]. First, the energies of all the virtual sub-carriers are determined which proceeds in a binary

hypothesis problem expressed as

$$\xi[k] = \left|\hat{\hat{Y}}[k]\right|^2 = \begin{cases} \left|S[k] + \ddot{Z}[k]\right|^2, & \mathcal{H}_0 \\ \left|\ddot{Z}[k]\right|^2, & \mathcal{H}_1, \end{cases} \quad (15)$$

for $k \in \llbracket 0, \Omega - 1 \rrbracket$, where $\ddot{\mathbf{Z}} = [\ddot{Z}[0], \ddot{Z}[1], \cdots, \ddot{Z}[\Omega - 1]]^{\text{T}}$ is the vector of colored noise on the virtual sub-carriers. It may be recognized that the components of $\mathbf{Z}$ are independent, accordingly, it can be inferred that components of $\ddot{\mathbf{Z}}$ are likewise independent. The null hypothesis, $\mathcal{H}_0$ specifies the activation of virtual sub-carrier, whilst the alternate hypothesis, $\mathcal{H}_1$ corresponds to non-activation. If the virtual sub-carrier is activated, the energy of the corresponding virtual sub-carrier would be higher than when there is merely noise on the virtual sub-carrier. Second, the energies $\boldsymbol{\xi} = [\xi[0], \xi[1], \cdots, \xi[\Omega - 1]]^{\text{T}}$ are sorted in the descending order, such that $\xi[\hat{\theta}_1] > \xi[\hat{\theta}_2] > \cdots > \xi[\hat{\theta}_\Omega]$, where the index of each component of $\boldsymbol{\xi}$ is given by $\hat{\theta}_k$ with $k \in \llbracket 1, \Omega \rrbracket$, which in vectorial form is given as $\hat{\boldsymbol{\theta}} = \{\hat{\theta}_1, \hat{\theta}_2, \cdots, \hat{\theta}_\Omega\}$. The first κ elements of $\hat{\boldsymbol{\theta}}$ corresponds to the indices of the virtual sub-carriers having the highest energies, therefore, $\hat{\boldsymbol{\theta}}$ is first cropped, such that it contains only κ components as $\hat{\boldsymbol{\theta}} = \{\hat{\theta}_1, \hat{\theta}_2, \cdots, \hat{\theta}_\kappa\}$ and then sorted in descending order conforming to the condition $\hat{\theta}_1 > \hat{\theta}_2 > \cdots > \hat{\theta}_\kappa$. Subsequently, $\hat{\boldsymbol{\theta}}$ is fed to the PT de-mapping algorithm to attain $\hat{\lambda}_1$. The constellation symbols modulated onto the active virtual sub-carriers are extracted as $\hat{\mathcal{X}}[k] = \hat{\hat{Y}}[\hat{\theta}_{k+1}]$, where $k \in \llbracket 0, \kappa - 1 \rrbracket$, which in vectorial form are given as $\hat{\boldsymbol{\mathcal{X}}} = [\hat{\mathcal{X}}[0], \hat{\mathcal{X}}[1], \cdots, \hat{\mathcal{X}}[\kappa - 1]]^{\text{T}}$. Using $\hat{\boldsymbol{\mathcal{X}}}$, $\hat{\lambda}_2$ are identified. For energy detector, only one multiplication per virtual sub-carrier is needed, therefore, the complexity is $\mathcal{O}(\Omega)$ which is considerably less than that of optimal ML detector.

2) LOW-COMPLEXITY DISJOINT MAXIMUM LIKELIHOOD DETECTOR

Unlike the optimal ML detector, the low-complexity ML detector determines $\hat{\boldsymbol{\theta}}$ and $\hat{\boldsymbol{\mathcal{X}}}$ modulated onto the active virtual sub-carriers successively is a disjoint manner. Assuming all the virtual sub-carriers are active, we ascertain the most likely alphabet modulated on each virtual sub-carrier. This is accomplished by appraising the inner product of $\hat{\hat{\mathbf{Y}}}$ and the alphabets, $\mathcal{S}$ from the PAM alphabet, $\mathcal{M}$. The dot product is expressed as

$$\alpha[k] = \arg \max_{\mathcal{S} \in \mathcal{M}} \{\langle \hat{\hat{Y}}[k]; \mathcal{S} \rangle\}, \quad (16)$$

for $k \in \llbracket 0, \Omega - 1 \rrbracket$, which in vectorial form is given as $\boldsymbol{\alpha} = [\alpha[0], \alpha[1], \cdots, \alpha[\Omega - 1]]^{\text{T}}$. Afterwards, κ virtual sub-carriers are identified which constitute $\hat{\boldsymbol{\theta}}$. To do so, the ML criterion

$$\gamma[k] = \alpha[k][\alpha[k] - \hat{\hat{Y}}[k]], \quad (17)$$

for $k \in \llbracket 0, \Omega - 1 \rrbracket$ is appraised resulting in $\boldsymbol{\gamma} = [\gamma[0], \gamma[1], \cdots, \gamma[\Omega - 1]]^{\text{T}}$. Ideally, for the active virtual sub-carriers, the ML decision metric (16) should be zero.

Thus, to determine $\hat{\boldsymbol{\theta}}$, the elements of $\boldsymbol{\gamma}$ are sorted in the ascending order as $\gamma[\hat{\theta}_1] < \gamma[\hat{\theta}_2] < \cdots < \gamma[\hat{\theta}_\Omega]$, where each component of $\boldsymbol{\gamma}$ is identified by $\hat{\theta}_k$ for $k \in [\![1, \Omega]\!]$ which in vectorial are given as $\hat{\boldsymbol{\theta}} = \{\hat{\theta}_1, \hat{\theta}_2, \cdots, \hat{\theta}_\Omega\}$. $\hat{\boldsymbol{\theta}}$ is identified by selecting first κ elements and sorting them in descending order, such that we have $\hat{\boldsymbol{\theta}} = \{\hat{\theta}_1, \hat{\theta}_2, \cdots, \hat{\theta}_\kappa\}$ which satisfy $\hat{\theta}_1 > \hat{\theta}_2 > \cdots > \hat{\theta}_\kappa$. Subsequently, the constellation symbols are obtained as $\hat{\mathcal{X}}[k] = \hat{Y}[\hat{\theta}_{k+1}]$ for $k \in [\![0, \kappa - 1]\!]$. $\hat{\boldsymbol{\theta}}$ is processed using the PT de-mapping to determine $\hat{\lambda}_1$, whereas, $\hat{\lambda}_2$ bits are attained using $\hat{\mathcal{X}}$. For low-complexity ML detector, two multiplications and one subtraction per virtual sub-carrier is needed, hence, the complexity is $\mathcal{O}(\Omega)$. The complexity of this detector is also significantly less than that of optimal ML detector.

Simulations performed in different settings have shown that both energy detector and the disjoint ML detector achieve the same performance while having the same order of complexity. Therefore, we will only show the performance results of the energy detector based receiver.

IV. PERFORMANCE ANALYSIS OF EO-OFDM-IM

In this section, we appraise the performances of EO-OFDM-IM in terms of SE, EE and BER. We consider LOS and time-dispersive propagation to evaluate BER. Classical O-OFDM and O-OFDM-IM approaches are considered as benchmarks. In order to highlight the benefits of each approach, the performance of each scheme is only compared to its direct counterpart having similar precept of achieving a non-negative signal available in the literature, e.g., DCEO-OFDM-IM is compared only with DCO-OFDM-IM and DCO-OFDM and not with ACO-OFDM-IM and ACO-OFDM.

A. SPECTRAL EFFICIENCY ANALYSIS
In this subsection, we analyze the SE of EO-OFDM-IM schemes and compare it with that of classical O-OFDM-IM approaches.[2] The total number of bits transmitted per EO-OFDM-IM symbol of duration T_s is λ as in (10). So, the data rate $R = \lambda/T_\mathrm{s}$ in bits/s for EO-OFDM-IM is appraised to be

$$R = \frac{\left\lfloor \log_2\binom{\Omega}{\kappa} \right\rfloor + \log_2(M^\kappa)}{T_\mathrm{s}}. \tag{18}$$

We recall that M is the cardinality of the alphabets modulated onto κ active virtual sub-carriers. Furthermore, we highlight that the base-band bandwidth requirements of DCEO-OFDM-IM and ACEO-OFDM-IM are different [3]. In [3], the authors elucidate the base-band bandwidth of real-valued O-OFDM signals. We can generalize the same analysis for base-band bandwidth for O-OFDM-IM and EO-OFDM-IM [12]. First, consider DCEO-OFDM-IM, for which the real-valued time-domain signal is attained after

adding the bias and subsequent clipping. The spectral leakage because of the clipping of residual negative excursions after addition of bias is negligible, thus, the base-band bandwidth, B for real-valued DCEO-OFDM-IM is almost $B \approx (\mathcal{N}/2)\Delta f = \mathcal{N}/2T_\mathrm{s}$. On the other hand, for ACEO-OFDM-IM, incurring to the antisymmetric property, all the negative amplitudes are clipped, therefore, the spectral leakage is significant, where all the complex-valued sub-carriers contains the harmonics because of clipping operation. Thus, the base-band bandwidth for ACEO-OFDM-IM is approximated to be $B \approx \mathcal{N}\Delta f = \mathcal{N}/T_\mathrm{s}$ [3]. Thus, the base-band bandwidths of EO-OFDM-IM schemes are

$$B \approx \begin{cases} \dfrac{\mathcal{N}}{2T_\mathrm{s}}, & \text{DCEO-OFDM-IM} \\[2mm] \dfrac{\mathcal{N}}{T_\mathrm{s}}, & \text{ACEO-OFDM-IM.} \end{cases} \tag{19}$$

Using (18) and (19), the SE $\eta = R/B$ in bits/s/Hz for EO-OFDM-IM approaches is calculated to be

$$\eta = \begin{cases} \dfrac{2\left(\left\lfloor \log_2\binom{\Omega}{\kappa} \right\rfloor + \log_2(M^\kappa)\right)}{\mathcal{N}}, & \text{DCEO-OFDM-IM} \\[4mm] \dfrac{\left\lfloor \log_2\binom{\Omega}{\kappa} \right\rfloor + \log_2(M^\kappa)}{\mathcal{N}}, & \text{ACEO-OFDM-IM.} \end{cases} \tag{20}$$

As aforementioned, κ can be varied to attain the peak η, therefore, we evaluate the approximate κ for peak η in Lemma 1.

Taking into consideration (i) that the base-band bandwidth requirement of ACEO-OFDM-IM is twice as that of DCEO-OFDM-IM; and (ii) Ω for DCEO-OFDM-IM is higher than that for ACEO-OFDM-IM, it can be anticipated using (20) that the SE of ACEO-OFDM-IM is substantially less than DCEO-OFDM-IM.

For O-OFDM-IM schemes, taking into account $\tilde{\Omega}$, $\tilde{\kappa}$ and considering that active complex-valued sub-carriers are modulated by $\tilde{M}$-ary QAM, the total number of bits transmitted in a symbol duration of $\tilde{T}_\mathrm{s}$ is equal to

$$\tilde{\lambda} = \left\lfloor \log_2\binom{\tilde{\Omega}}{\tilde{\kappa}} \right\rfloor + \log_2(\tilde{M}^{\tilde{\kappa}}), \tag{21}$$

culminating in data rate $\tilde{R} = \tilde{\lambda}/\tilde{T}_\mathrm{s}$ in bits/s of

$$\tilde{R} = \frac{\left\lfloor \log_2\binom{\tilde{\Omega}}{\tilde{\kappa}} \right\rfloor + \log_2(\tilde{M}^{\tilde{\kappa}})}{\tilde{T}_\mathrm{s}}. \tag{22}$$

Using the same principle as in [3], the base-band bandwidth requirements for O-OFDM-IM schemes are evaluated to be

$$\tilde{B} \approx \begin{cases} \dfrac{\mathcal{N}}{2\tilde{T}_\mathrm{s}}, & \text{DCO-OFDM-IM} \\[2mm] \dfrac{\mathcal{N}}{\tilde{T}_\mathrm{s}}, & \text{ACO-OFDM-IM.} \end{cases} \tag{23}$$

---

[2]We do not consider CP for assessment of SE in the sequel. However, using CP of the same length for all approaches would equitably lessen the absolute SE.

resulting in SE $\tilde{\eta} = \tilde{R}/\tilde{B}$ of

$$\tilde{\eta} = \begin{cases} \dfrac{2\left(\left\lfloor \log_2\left(\frac{\tilde{\Omega}}{\tilde{\kappa}}\right)\right\rfloor + \log_2(\tilde{M}^{\tilde{\kappa}})\right)}{\mathcal{N}}, & \text{DCO-OFDM-IM} \\[4mm] \dfrac{\left\lfloor \log_2\left(\frac{\tilde{\Omega}}{\tilde{\kappa}}\right)\right\rfloor + \log_2(\tilde{M}^{\tilde{\kappa}})}{\mathcal{N}}, & \text{ACO-OFDM-IM.} \end{cases} \quad (24)$$

in bits/s/Hz for O-OFDM-IM schemes. Since $\Omega > \tilde{\Omega}$ and $\kappa > \tilde{\kappa}$ for peak SE, then, using PT it can be discerned that the amount of index domain information conveyed by EO-OFDM-IM is higher than that of O-OFDM-IM, proceeding in higher η relative to $\tilde{\eta}$.

For O-OFDM, considering $\dot{\Omega}$ complex-valued sub-carriers modulated with $\dot{M}$-ary QAM, the number of bits, $\dot{\lambda}$ transmitted per O-OFDM symbol of duration $\dot{T}_s$ is evaluated to be $\dot{\lambda} = \tilde{\Omega}\log_2(\tilde{M})$ proceeding in data rate $\dot{R} = \dot{\lambda}/\dot{T}_s = \tilde{\Omega}\log_2(\tilde{M})/\dot{T}_s$ bits/s. As evaluated in [3], the base-band bandwidth requirements for DCO-OFDM and ACO-OFDM are respectively equal to $\dot{B} \approx \mathcal{N}/2\dot{T}_s$ and $\dot{B} \approx \mathcal{N}/\dot{T}_s$, then, the SE $\dot{\eta} = \dot{R}/\dot{B}$ of O-OFDM schemes in bits/s/Hz is

$$\dot{\eta} = \begin{cases} \dfrac{2\tilde{\Omega}\log_2(\tilde{M})}{\mathcal{N}}, & \text{DCO-OFDM} \\[4mm] \dfrac{\tilde{\Omega}\log_2(\tilde{M})}{\mathcal{N}}, & \text{ACO-OFDM.} \end{cases} \quad (25)$$

Lemma 1: Considering Ω, the peak SE for EO-OFDM-IM schemes employing alphabets $\mathcal{M}$ of cardinality M for IM virtual sub-carriers is realized if the number of active virtual sub-carriers are approximately

$$\kappa_{\text{approx}} \approx \left\lfloor \frac{M\Omega}{M+1} \right\rfloor. \quad (26)$$

Proof: For given $\{\Omega, M\}$, η changes for κ. Since the maximization of η is correlated with maximization of λ, thus, the objective is to find κ which maximizes (10). So, considering (10) and discarding the floor function, the following inequality must hold

$$\lambda \leq \log_2\binom{\Omega}{\kappa} + \log_2(M^{\kappa}). \quad (27)$$

Taking the derivative of (27) with respect to κ, one obtains

$$\frac{d\lambda}{d\kappa} \leq \frac{\psi_{\Omega-\kappa} - \psi_{\kappa} + \log(M)}{\log(2)}, \quad (28)$$

where $\psi_m = \sum_{k=1}^{m}\frac{1}{k}$ is the mth harmonic number which is approximated as $\psi_m \approx \log(m) + \epsilon$, where ϵ is the Euler–Mascheroni constant. Substituting this approximation in (28) and setting the derivative $d\lambda/d\kappa$ equal to zero, we obtain

$$\kappa \leq \frac{M\Omega}{M+1}, \quad (29)$$

after simple mathematical manipulation. By reintroducing the floor function, the approximate value of κ, i.e., κ_{approx} is obtained as in (26). ∎

Following similar steps as in the proof of Lemma 1, the approximate active complex-valued sub-carriers for
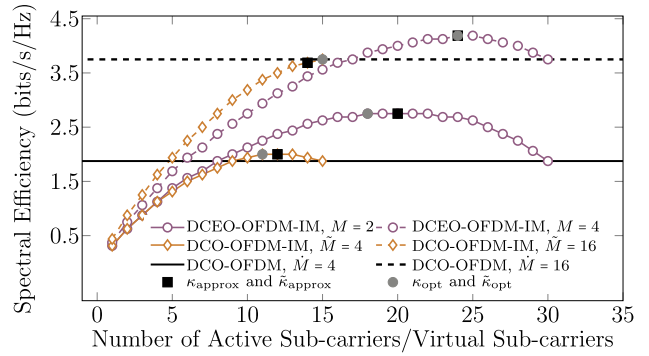
FIGURE 5. SE evolution of DCEO-OFDM-IM and DCO-OFDM-IM with respect to the number of active sub-carriers/virtual sub-carriers.
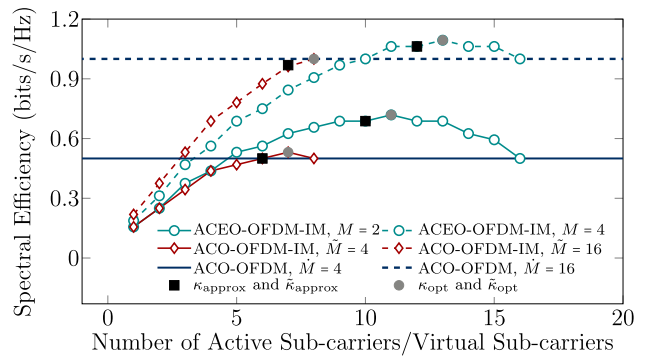
FIGURE 6. SE evolution of ACEO-OFDM-IM and ACO-OFDM-IM with respect to the number of active sub-carriers/virtual sub-carriers.

O-OFDM-IM which maximizes $\tilde{\eta}$ with parameters $\{\tilde{\Omega}, \tilde{M}\}$ are appraised to be

$$\tilde{k}_{\text{approx}} \approx \left\lfloor \frac{\tilde{M}\tilde{\Omega}}{\tilde{M}+1} \right\rfloor. \quad (30)$$

Note that for O-OFDM schemes the maximum $\dot{\eta}$ is same as in (25). The approximate value of κ (resp. $\tilde{\kappa}$) as in (26) (resp. (30)) may or may not be the optimal value of κ (resp. $\tilde{\kappa}$); which is denoted by κ_{opt} (resp. $\tilde{\kappa}_{\text{opt}}$). κ_{opt} (resp. $\tilde{\kappa}_{\text{opt}}$) attributes to the minimum number of active virtual sub-carriers (resp. complex-valued sub-carriers) for which we obtain maximum SE. For κ_{opt} (resp. $\tilde{\kappa}_{\text{opt}}$), lesser frequency resources may be employed resulting in better EE. The marginal disparity between the optimal and approximate values is due to the floor function which was dropped to evaluate (26) and (30).

Fig. 5 and 6 respectively illustrate the progression of the spectral efficiencies of DCEO-OFDM-IM and ACEO-OFDM with respect to κ by adopting PAM alphabets of cardinalities $M = \{2, 4\}$. The SE evolution of classical O-OFDM-IM with respect to $\tilde{\kappa}$ using $\tilde{M} = \{4, 16\}$ QAM, and the SE of O-OFDM using $\dot{M} = \{4, 16\}$ QAM is presented as a benchmark. We consider $\mathcal{N} = 32$ for all approaches. κ_{opt}, $\tilde{\kappa}_{\text{opt}}$, κ_{approx} and $\tilde{\kappa}_{\text{approx}}$ are also indicated in Figs. 5 and 6. For $\{M, \tilde{M}, \dot{M}\} = \{2, 4, 4\}$, the obtainable peak SE for DCEO-OFDM-IM,

DCO-OFDM-IM and DCO-OFDM is 2.75 bits/s/Hz, 2 bits/s/Hz and 1.875 bits/s/Hz, respectively indicating that DCEO-OFDM-IM offers approximately 37.5% and 46.7% higher SE than DCO-OFDM-IM and DCO-OFDM, respectively. Similarly, the attainable peak SE of ACEO-OFDM-IM, ACO-OFDM-IM and ACO-OFDM with identical parameters is 0.7188 bits/s/Hz, 0.5313 bits/s/Hz and 0.5 bits/s/Hz. Thus, ACEO-OFDM-IM gains up to 35.3% and 43.8% in SE over ACO-OFDM-IM and ACO-OFDM. Nonetheless, for higher alphabet cardinalities, the peak SE improvement afforded by DCEO-OFDM-IM and ACEO-OFDM-IM over other counterparts is merely 11.7% and 9.4%, respectively; which is marginal. This indicates that EO-OFDM-IM schemes are ideal for low alphabet cardinalities.

B. ENERGY EFFICIENCY ANALYSIS

In this subsection, we investigate the granularity for EE/SE trade-off offered by EO-OFDM-IM in LOS optical wireless propagation channel. For a given SE, the EE is appraised by determining the required signal-to-noise ratio (SNR) per bit $E_{b_{(elec)}}/N_0 = \mathcal{N}\sigma^2 T_s/\lambda N_0$ for target BER of 10^{-3}. We consider $\mathcal{N} = 32$, $M \in \{2, 4\}$ for EO-OFDM-IM schemes and $\tilde{M} \in \{4, 16\}$ for O-OFDM-IM approaches. The bias values for DCEO-OFDM-IM and DCO-OFDM-IM are adapted such that target BER is attained without increasing required $E_{b_{(elec)}}/N_0$. Note that if higher than needed values of bias are used, $E_{b_{(elec)}}/N_0$ increases as $E_{b_{(elec)}}$ increases. On the contrary, if lower bias values are used, the clipping distortion would be substantial which would increase the required $E_{b_{(elec)}}/N_0$ to obtain the target BER.

From Figs. 5 and 6, we can gather specific peculiarities of classical schemes, which influence their EE. First, to reach the same SE as that of EO-OFDM-IM, O-OFDM-IM and O-OFDM require alphabets with higher cardinalities, which are inherently less energy-efficient. This behavior of classical approaches would become apparent in the subsequent section where we analyze the BER performances of different schemes. Second, the number of active complex-valued sub-carriers for O-OFDM-IM, $\tilde{\kappa}$ are generally equal to $\tilde{\Omega}$ to attain peak $\tilde{\eta}$ (cf. Figs. 5 and 6). This entails that the sparsity of the frequency-domain signal, $\dot{X}$ (and in turn X) is not substantial. Note that for EO-OFDM-IM, the number of active virtual sub-carriers, κ is consistently less than Ω, however, it is difficult to ascertain the sparsity of frequency-domain signal, $\dot{X}$ after in-phase and quadrature consolidation as it depends on $\boldsymbol{\theta}$.

Figs. 7 and 8 illustrate the EE/SE trade-off for EO-OFDM-IM and O-OFDM-IM approaches. For DCEO-OFDM-IM, κ varies as $\kappa \in [\![1, 20]\!]$ for $M = 2$ and $\kappa \in [\![1, 24]\!]$ for $M = 4$ proceeding in spectral efficiencies of $\eta = \{0.3125 \rightarrow 2.75\}$ bits/s/Hz and $\eta = \{0.375 \rightarrow 4.1875\}$ bits/s/Hz, respectively. Whereas, for DCO-OFDM-IM, the spectral efficiencies vary as $\tilde{\eta} = \{0.3125 \rightarrow 2\}$ bits/s/Hz (for $\tilde{M} = 4$) and $\tilde{\eta} = \{0.4375 \rightarrow 3.75\}$ bits/s/Hz (for $\tilde{M} = 16$) with corresponding $\tilde{\kappa} \in [\![1, 11]\!]$ and $\tilde{\kappa} \in [\![1, 15]\!]$. $\dot{\eta}$ for DCO-OFDM with $\{\mathcal{N}, \dot{M}\} = \{32, 4\}$ and $\{\mathcal{N}, \dot{M}\} = \{32, 16\}$ is 1.875 bits/s/Hz
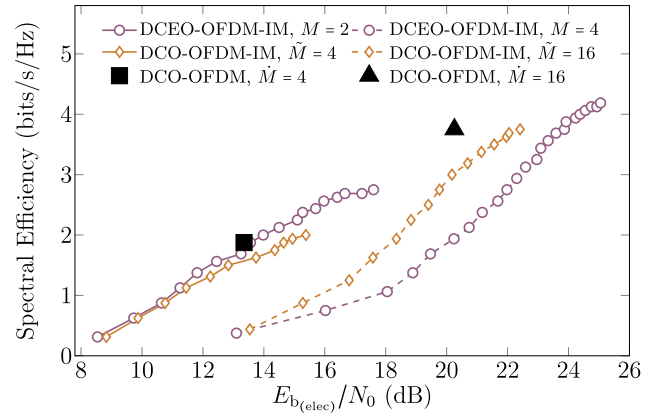
FIGURE 7. The evolution of required $E_{b_{(elec)}}/N_0$ for DCEO-OFDM-IM and DCO-OFDM-IM with respect to η and $\tilde{\eta}$ for target BER of 10^{-3}. The EE versus SE performance of DCO-OFDM with $\dot{M} \in \{4, 16\}$ is also presented as benchmark.

and 3.75 bits/s/Hz. On the other hand, for ACEO-OFDM-IM, the spectral efficiencies are $\eta = \{0.1563 \rightarrow 0.7188\}$ bits/s/Hz when $M = 2$ and $\eta = \{0.1875 \rightarrow 1.0938\}$ bits/s/Hz when $M = 4$ are realized for $\kappa \in [\![1, 11]\!]$ and $\kappa \in [\![1, 13]\!]$, respectively. For ACO-OFDM-IM, $\tilde{\kappa}$ ranges between $\tilde{\kappa} \in [\![1, 7]\!]$ when $\tilde{M} = 4$ and $\tilde{\kappa} \in [\![1, 8]\!]$ when $\tilde{M} = 16$, offering spectral efficiencies of $\tilde{\eta} = \{0.1563 \rightarrow 0.5313\}$ bits/s/Hz and $\tilde{\eta} = \{0.2188 \rightarrow 1\}$ bits/s/Hz, respectively. Considering $\{\mathcal{N}, \dot{M}\} = \{32, 4\}$ and $\{\mathcal{N}, \dot{M}\} = \{32, 16\}$, $\dot{\eta}$ for ACO-OFDM is respectively 0.5 bits/s/Hz and 1 bits/s/Hz. From Figs. 7 and 8, we recognize the following concrete advantages of EO-OFDM-IM over counterparts: (i) it yields an extended granularity for EE/SE trade-off, e.g., 20 operating points for DCEO-OFDM-IM (compared to 11 for DCO-OFDM-IM) when $M = 2$, which is favorable for energy-efficient IoT OWS and/or high data-rate OWS; (ii) it is more energy-efficient than classical O-OFDM-IM, e.g., DCEO-OFDM-IM is more energy-efficient than DCO-OFDM-IM for spectral efficiencies > 1 bits/s/Hz; and (iii) it possesses the potential of realizing higher SE than other alternatives while maintaining EE. We also notice that O-OFDM-IM provides limited EE/SE trade-off with lower EE, while O-OFDM is incapable of affording any EE/SE trade-off.

Figs. 7 and 8 also illustrate one notable limitation of EO-OFDM-IM, i.e., even though these schemes can attain higher SE than O-OFDM-IM and O-OFDM, however, when the alphabet cardinality increases, EO-OFDM-IM loses its EE. This behavior is similar to what we observe for DCO-FOFDM-IM [12]. Cognizant of the fact that for higher alphabet cardinalities, the increase in SE for EO-OFDM-IM over other alternatives is minimal (cf. Fig. 5 and 6) coupled with the fact that they lose their EE, the region of interest for EO-OFDM-IM is within the SE range which is attained when $M = 2$. We reiterate that within the region of interest, the attainable SE of EO-OFDM-IM is much higher than O-OFDM-IM or O-OFDM. Thus, with DCEO-OFDM-IM,
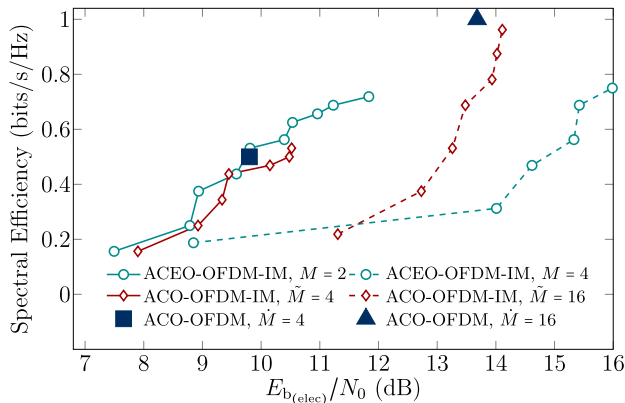
FIGURE 8. The evolution of required $E_{b_{(elec)}}/N_0$ for ACEO-OFDM-IM and ACO-OFDM-IM with respect to η and $\tilde{\eta}$ for target BER of 10^{-3}. The EE versus SE performance of ACO-OFDM with $\dot{M} \in \{4, 16\}$ is also presented as benchmark.

we can effectively target low SE and high EE IoT communication and mid-to-high spectral efficiencies, whereas, ACEO-OFDM-IM can be used where low spectral efficiencies with high EE are needed.

C. BIT ERROR RATE ANALYSIS

In this section, we analyze the BER performances. Firstly, we present the BER performance of EO-OFDM-IM schemes for diverse spectral efficiencies which can be targeted within the region of interest. Secondly, we appraise the BER performances for EO-OFDM-IM schemes in the low and mid-to-high SE regions suitable for IoT applications and indoor OWS. The BER performance is evaluated in the LOS optical wireless channel and time dispersive channel. The impulse response of time dispersive channel obtained via ceiling bounce model [22] is given by

$$h(t) = \zeta \frac{\varsigma^2}{(t + \varsigma)^2} u(t), \tag{31}$$

where $\varsigma = 2H_{\text{ceil}}/c$ with H_{ceil} and c being the ceiling height and the speed of light, respectively. ζ is the optical path loss normalized to unity. The root mean square delay spread of the channel $\Delta\tau$ is linked to ς as $(\varsigma/12)\sqrt{13/11}$ and is set at 10 ns. The data rate considered is 50Mbits/s.

Figs. 9 and 10 depict the BER performances for DCEO-OFDM-IM and ACEO-OFDM-IM for different spectral efficiencies within the region of interest for both energy detector receiver and disjoint ML detector receiver. The spectral efficiencies analyzed for DCEO-OFDM-IM are $\eta = \{0.3125, 1.5625, 2.375, 2.75\}$ bits/s/Hz which are achieved using $\kappa = \{1, 6, 12, 18\}$, respectively. For ACEO-OFDM-IM, we consider $\kappa = \{1, 5, 8, 11\}$ following spectral efficiencies of $\eta = \{0.1563, 0.5313, 0.6563, 0.7188\}$ bits/s/Hz. It may be noticed the performance of both detectors is exactly the same. These results indicate that we can target a range of applications involving different spectral and/or energy efficiencies. Furthermore, $\kappa = 1$ for DCEO-OFDM-IM
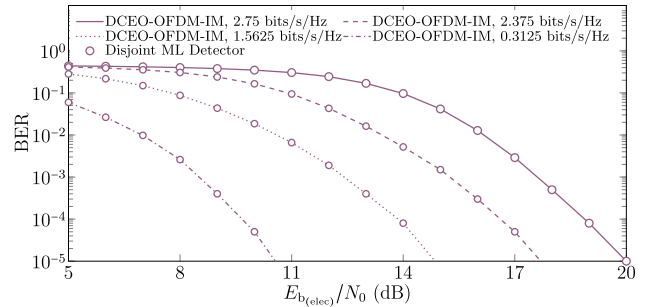

FIGURE 9. BER performance of DCEO-OFDM-IM for $\eta = \{0.3125, 1.5625, 2.375, 2.75\}$ bits/s/Hz for energy detector receiver (lines) and disjoint ML detector receiver (markers).
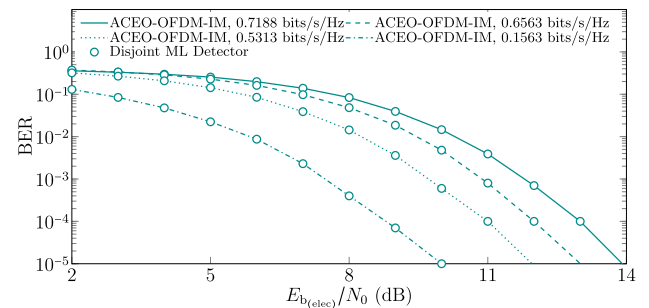

FIGURE 10. BER performance ACEO-OFDM-IM for $\eta = \{0.1563, 0.5313, 0.6563, 0.7188\}$ bits/s/Hz for energy detector receiver (lines) and disjoint ML detector receiver (markers).

corresponds to DC-FPSK we proposed in [19] for energy-efficient IoT communications.

Next, in Fig. 11, we provide the BER performance of DCEO-OFDM-IM and DCO-OFDM-IM considering LOS and time dispersive propagation for low SE of 0.625 bits/s/Hz; which is pertinent for IoT based OWS. For an impartial comparison, a bias of 3.8 dB is adopted for both approaches. Because of DCO-OFDM's inability for EE/SE trade-off, it cannot attain 0.625 bits/s/Hz. We observe that for low SE region, the performance of both schemes in both LOS and time dispersive propagation is practically identical. The BER performance of DCEO-OFDM-IM is similar to that of DCO-OFDM-IM for spectral efficiencies < 1 bits/s/Hz (cf. Fig. 7). For spectral efficiencies > 1 bits/s/Hz, the BER performance of DCEO-OFDM-IM tends to become more energy efficient than DCO-OFDM-IM.

Fig. 12 compares the BER performance of DCEO-OFDM-IM with that of DCO-OFDM-IM and DCO-OFDM in a high spectral region. The reference SE we consider is $\eta = 2.75$ bits/s/Hz, i.e., the peak SE that can be attained in the region of interest for DCEO-OFDM-IM when $\{\mathcal{N}, M, \kappa\} = \{32, 2, 20\}$. Since the counterparts, that are, DCO-OFDM-IM and DCO-OFDM, cannot attain the reference SE with lowest alphabet, i.e., $\tilde{M} = \dot{M} = 4$, hence we consider alphabets for the higher cardinalities, such that the SE attained by these approaches is close to the reference SE. For DCO-OFDM-IM and DCO-OFDM, we consider $\{\mathcal{N}, \tilde{M}, \tilde{\kappa}\} = \{32, 16, 8\}$ and $\{\mathcal{N}, \dot{M}\} = \{16, 16\}$, respectively. With these parameters,
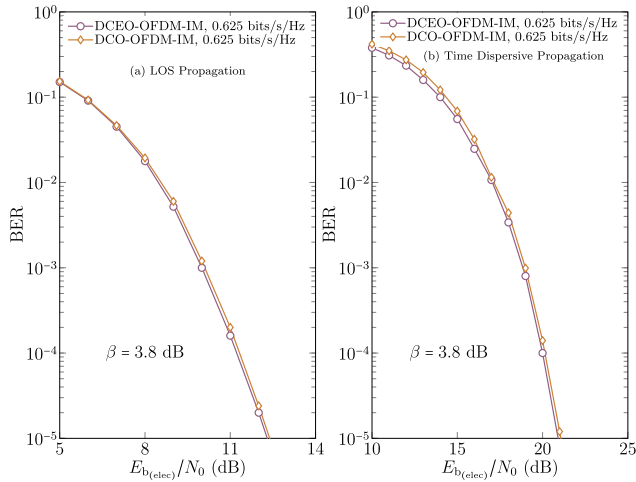
FIGURE 11. BER performance comparison of DCEO-OFDM-IM and DCO-OFDM-IM for a reference SE of 0.625 bits/s/Hz considering (a) LOS propagation; and (b) time dispersive propagation.
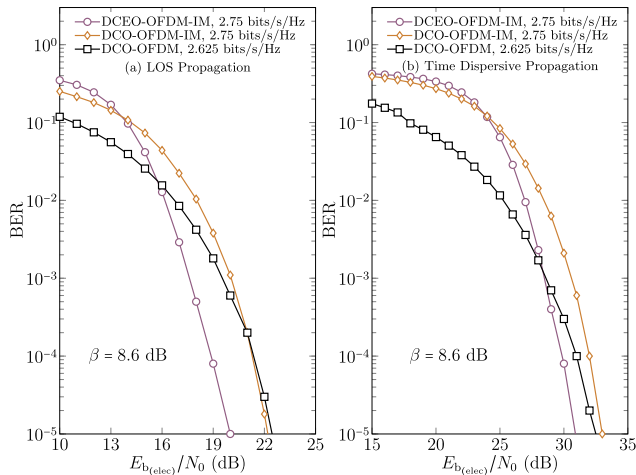

FIGURE 13. BER performance comparison of ACEO-OFDM-IM and ACO-OFDM-IM for a reference SE of 0.25 bits/s/Hz considering. (a) LOS propagation; and (b) time dispersive propagation.

FIGURE 12. BER performance comparison of DCEO-OFDM-IM, DCO-OFDM-IM and DCO-OFDM for a reference SE of 2.75 bits/s/Hz considering. (a) LOS propagation; and (b) time dispersive propagation.

respectively for ACEO-OFDM-IM and ACO-OFDM-IM to obtain the reference SE. We can observe that for low reference SE, the performance of both ACEO-OFDM-IM and ACO-OFDM-IM is comparable in both LOS and time dispersive propagation. Next, we consider a high reference SE of 0.7188 bits/s/Hz in the region of interest, which is obtained when $\{\mathcal{N}, M, \kappa\} = \{32, 2, 11\}$ for ACEO-OFDM-IM. The closest SE possible from ACO-OFDM-IM is 0.6875 bits/s/Hz which is 4.35% less than the reference and is obtained when $\{\mathcal{N}, \tilde{M}, \tilde{\kappa}\} = \{32, 16, 4\}$, whereas, for ACO-OFDM, the SE close to the reference is 0.75 bits/s/Hz attained when $\{\mathcal{N}, \dot{M}\} = \{32, 16\}$ which is 4.16% higher than the reference value. The BER performance considering LOS and time dispersive propagation with the above parameters are presented in Fig. 14. We observe that the performance of ACEO-OFDM-IM for high $E_{b(elec)}/N_0$ is approximately 2 dB better than the counterparts at BER of 10^{-3}. Moreover, ACO-OFDM-IM performs worst in both LOS and time dispersive propagation because alphabet with high order cardinality is used.

From the results presented in Fig. 11, 12, 13 and 14, we gather that EO-OFDM-IM schemes are better not merely for low spectral efficiencies within the region of interest, where they offer comparable performance to that of classical counterparts, but likewise for higher spectral efficiencies in the region of interest, where they manifest better EE over alternatives. We also highlight that proposed approaches can be adopted for low SE IoT application, while DCEO-OFDM-IM can also be employed for applications demanding mid-to-high spectral efficiencies.

V. PROPOSED ENHANCED O-OFDM DUAL MODE SCHEMES

For EO-OFDM-IM schemes, we recognize that (i) the SE gain over classical approaches is less when we use higher-order alphabets; and (ii) the EE is viable for low

the SE attained DCO-OFDM-IM is 2.75 bits/s/Hz, while for DCO-OFDM it is 2.625 bits/s/Hz which is almost 4.55% less than the reference SE. A bias of 8.6 dB is considered for all the approaches. We can observe that the performance of DCEO-OFDM-IM is better than other counterparts for high $E_{b(elec)}/N_0$ in both LOS and time dispersive propagation primarily because it utilizes the alphabet with the lowest cardinality which is intrinsically energy-efficient. Furthermore, it seems that DCO-OFDM-IM has the worst performance among all the examined approaches, however, it is pointed out that in given results (cf. Fig. 12), the SE of DCO-OFDM-IM is slightly higher than that of DCO-OFDM.

Fig. 13 illustrates the BER comparison of ACEO-OFDM-IM and ACO-OFDM-IM for a low reference SE of 0.25 bits/s/Hz in the region of interest. We use the parameters $\{\mathcal{N}, M, \kappa\} = \{32, 2, 2\}$ and $\{\mathcal{N}, \tilde{M}, \tilde{\kappa}\} = \{32, 4, 2, 2\}$
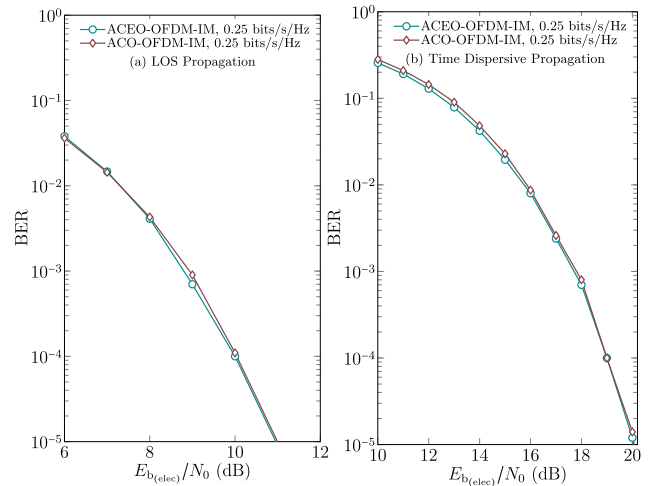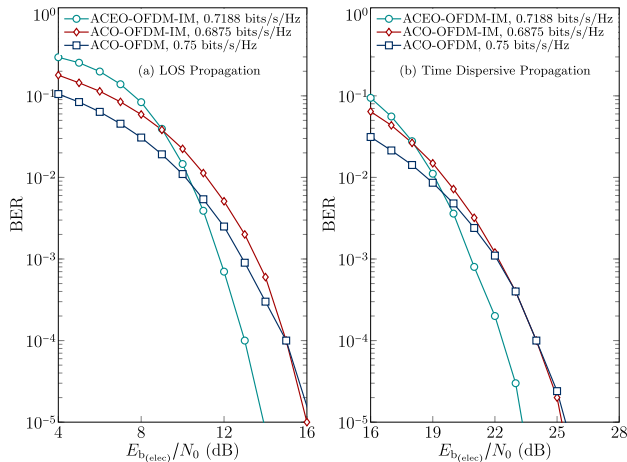
FIGURE 14. BER performance comparison of ACEO-OFDM-IM, ACO-OFDM-IM and ACO-OFDM for a reference SE of 0.7188 bits/s/Hz considering. (a) LOS propagation; and (b) time dispersive propagation.
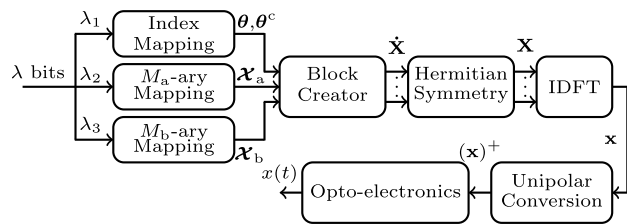

FIGURE 15. Generalized transmitter architecture for EO-OFDM-DM schemes.

cardinality alphabets. Thus, as aforementioned, only low order alphabets can be used for EO-OFDM-IM making it impossible to attain the same SE as that O-OFDM when $\dot{M} = 16$. Nonetheless, O-OFDM-IM approaches performs better than EO-OFDM-IM schemes, but are yet worse than O-OFDM. To surmount this limitation of EO-OFDM-IM, we propose the DM counterpart of EO-OFDM-IM. In the next section, we succinctly present the transceiver design.

A. TRANSMITTER ARCHITECTURE

The transmitter configuration of ECO-OFDM-DM transmitter is depicted in Fig. 15. The equiprobable bit sequence is parsed into three distinct bit sequences of length λ_1, λ_2 and λ_3. λ_1 bits are for IM which determines the SAP of length κ, i.e., $\theta = \{\theta_1, \theta_2, \cdots, \theta_\kappa\} \in \Theta$ and are equal to

$$\lambda_1 = \left\lfloor \log_2 \binom{\Omega}{\kappa} \right\rfloor. \tag{32}$$

The bit sequence of length λ_2 is utilized to generate κ symbols, $\mathcal{X}_a = [\mathcal{X}_a[0], \mathcal{X}_a[1], \cdots, \mathcal{X}_a[\kappa - 1]]^T$ from alphabet $\mathcal{M}_a$ of cardinality M_a to be modulated onto the virtual sub-carriers determined by θ. Thus, λ_2 is equal to

$$\lambda_2 = \log_2(M_a^\kappa). \tag{33}$$

λ_3 bits are exploited to generate $\Omega - \kappa$ symbols, $\mathcal{X}_b = [\mathcal{X}_b[0], \mathcal{X}_b[1], \cdots, \mathcal{X}_b[\Omega - \kappa - 1]]^T$ from constellation $\mathcal{M}_b$

of cardinality M_b to be modulated on the virtual sub-carriers with indices $\theta^c = \{\theta_1^c, \theta_2^c, \cdots, \theta_{\Omega-\kappa}^c\}$, where θ^c is the complement of set θ, such that $\theta \cap \theta^c = \phi$ and $\theta \cup \theta^c = \Theta$. λ_3 bits are given by

$$\lambda_3 = \log_2(M_b^{\Omega-\kappa}). \tag{34}$$

Thus, the total number of bits in EO-OFDM-DM symbol of duration T_s is equal to

$$\lambda = \left\lfloor \log_2 \binom{\Omega}{\kappa} \right\rfloor + \log_2(M_a^\kappa) + \log_2(M_b^{\Omega-\kappa}). \tag{35}$$

For EO-OFDM-DM, we consider two distinct constellations, $\mathcal{M}_a$ and $\mathcal{M}_b$ of cardinalities M_a and M_b, respectively for IM and non-IM virtual sub-carriers. For simplicity, we consider both constellation alphabets belong to PAM constellation, and the distinct aspect is the average symbol energy. For example, when $M_a = M_b = 2$, then, we have $\mathcal{M}_a \in \{-3, 3\}$ and $\mathcal{M}_b \in \{-1, 1\}$, where the average symbol energy of constellation alphabets from $\mathcal{M}_a$ is $E_{\text{avg}}^\kappa = 3(M_a^2 - 1)$, whilst the average symbol energy of constellation alphabets, $\mathcal{M}_b$ is $E_{\text{avg}}^{\Omega-\kappa} = (M_b^2 - 1)/3$.

The vector $\mathbf{S} = [S[0], S[1], \cdots, S[\Omega - 1]]^T$ having Ω virtual sub-carriers is obtained using θ, θ^c, $\mathcal{X}_a$ and $\mathcal{X}_b$ as:

$$S[k] = \begin{cases} \mathcal{X}_a[k], & k \in \theta \\ \mathcal{X}_b[k], & k \in \theta^c \end{cases}, \quad k \in [\![0, \Omega - 1]\!]. \tag{36}$$

Afterwards, using $\mathbf{S}$ and $\mathbf{X}$, $\mathbf{x}$ is achieved the same way as for EO-OFDM-IM. The signal space of EO-OFDM-DM considering $\mathcal{M}_a \in \{-3, 3\}$ and $\mathcal{M}_b \in \{-1, 1\}$ is depicted in Fig. 16. Note that the vector $\dot{\mathbf{X}}$ representing the signal space is also realized in the same way as for EO-OFDM-IM (cf. Section III). It may be noticed that the null point in the signal space is not possible for EO-OFDM-DM approaches as all the virtual sub-carriers are modulated (cf. Fig. 16).

The average electrical symbol energy and average symbol power of bipolar time-domain $\mathbf{x}$ is $\mathbb{E}\left\{\|x_k\|^2\right\} = \mathbb{E}\left\{\sum_{k=0}^{\mathcal{N}-1} x_k^2\right\} = 2(\kappa E_{\text{avg}}^\kappa + (\Omega - \kappa)E_{\text{avg}}^{\Omega-\kappa})$ and $\sigma_x^2 = \mathbb{E}\left\{\|x_k\|^2\right\}/\mathcal{N}$, respectively. Like in DCEO-OFDM-IM,
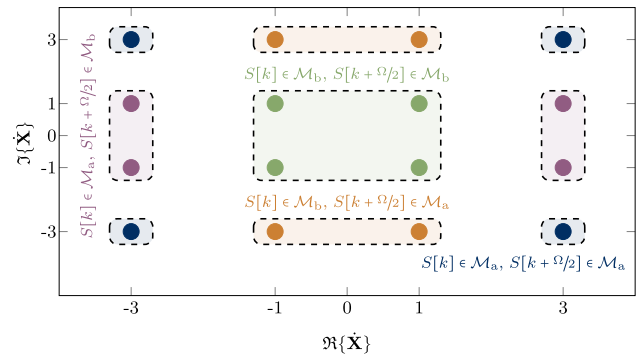

FIGURE 16. Signal space for EO-OFDM-DM schemes for $\mathcal{M}_a \in \{-3, 3\}$ and $\mathcal{M}_b \in \{-1, 1\}$, i.e., $M_a = M_b = 2$ and $k \in [\![0, \Omega/2 - 1]\!]$.
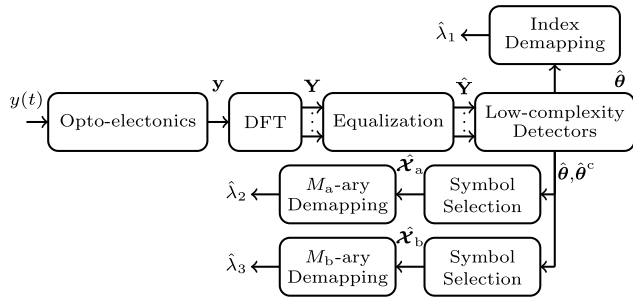
FIGURE 17. Generalized receiver architecture for EO-OFDM-DM schemes.

a bias equal to $\beta = \mu\sigma_x$ and subsequent zero level clipping of negative amplitude excursions is employed to realize $(\mathbf{x})^+$. For ACEO-OFDM-DM, the negative excursions of the time-domain signal $\mathbf{x}$ are clipped resulting in $(\mathbf{x})^+$. The analog electrical intensity waveform, $x(t)$ attained after CP addition and opto-electronic processing, is transmitted to the optical wireless channel using an LED.

The average symbol energy of $(\mathbf{x})^+$ evaluated as $\mathbb{E}\left\{\|x_k^+\|^2\right\}$ is equal to $2\kappa E_{\mathrm{avg}}^\kappa + (\Omega - \kappa)E_{\mathrm{avg}}^{\Omega-\kappa} + \mathcal{N}\mu^2$ and $\kappa E_{\mathrm{avg}}^\kappa + (\Omega - \kappa)E_{\mathrm{avg}}^{\Omega-\kappa}$ for DCEO-OFDM-DM and ACEO-OFDM-DM, respectively. The average symbol power of $(\mathbf{x})^+$ for EO-OFDM-DM schemes is equal to $\sigma^2 = \mathbb{E}\left\{\|x_k^+\|^2\right\}/\mathcal{N}$.

B. RECEIVER ARCHITECTURES

In EO-OFDM-IM, the virtual sub-carriers are active or not active, however, in EO-OFDM-DM all the virtual sub-carriers have some alphabets modulated on them. Therefore, the detectors presented in Section III B require minute adjustments to be adaptable with EO-OFDM-DM. At the receiver, the vector $\hat{\hat{\mathbf{Y}}}$ is realized as in EO-OFDM-IM. A generalized configuration of EO-OFDM-DM receiver is presented in Fig. 17 and fundamental differences for the detectors are outlined in the following. In EO-OFDM-DM, the detectors have to determine $\hat{\boldsymbol{\theta}}$, $\hat{\boldsymbol{\theta}}^{\mathrm{c}}$, $\hat{\boldsymbol{\mathcal{X}}}_{\mathrm{a}}$ and $\hat{\boldsymbol{\mathcal{X}}}_{\mathrm{b}}$.

1) ENERGY DETECTOR

In EO-OFDM-IM the energies of active virtual sub-carriers under ideal circumstances are E_{avg}, whereas energies of the non-active virtual sub-carriers is zero. In EO-OFDM-DM, the κ IM virtual sub-carriers carrying alphabets from $\mathcal{M}_{\mathrm{a}}$ have average symbol energies equal to E_{avg}^κ, whereas, the remaining $\Omega - \kappa$ non-IM virtual sub-carriers modulated by $\mathcal{M}_{\mathrm{b}}$ have average symbol energies $E_{\mathrm{avg}}^{\Omega-\kappa}$. Therefore, the detection problem is to discriminate between the virtual sub-carriers having average symbol energies E_{avg}^κ or $E_{\mathrm{avg}}^{\Omega-\kappa}$. By appraising the energies of all virtual sub-carrier as $\xi[k] = |\hat{\hat{Y}}[k]|^2$ for $k \in [\![0, \Omega - 1]\!]$, we obtain $\boldsymbol{\xi} = [\xi[0], \xi[1], \cdots, \xi[\Omega - 1]]^{\mathrm{T}}$. Using $\boldsymbol{\xi}$, $\hat{\boldsymbol{\theta}} = \{\hat{\theta}_1, \hat{\theta}_2, \cdots, \hat{\theta}_\Omega\}$ is obtained adhering to the same procedure as in EO-OFDM-IM. We recall that $\hat{\boldsymbol{\theta}}$ represents the indices of the components of $\boldsymbol{\xi}$ sorted in descending order. Note that the energy of

alphabets on κ IM virtual sub-carriers E_{avg}^κ is higher than that of the alphabets on $\Omega - \kappa$ non-IM virtual sub-carriers, i.e., $E_{\mathrm{avg}}^\kappa > E_{\mathrm{avg}}^{\Omega-\kappa}$, therefore, the first κ components of $\hat{\boldsymbol{\theta}}$ sorted in descending order gives the SAP, $\hat{\boldsymbol{\theta}} = \{\hat{\theta}_1, \hat{\theta}_2, \cdots, \hat{\theta}_\kappa\}$. The last $\Omega - \kappa$ components of $\hat{\boldsymbol{\theta}}$ yields the indices of non-IM virtual sub-carriers, i.e., $\hat{\boldsymbol{\theta}}^{\mathrm{c}} = \{\hat{\theta}_1^{\mathrm{c}}, \hat{\theta}_2^{\mathrm{c}}, \cdots, \hat{\theta}_{\Omega-\kappa}^{\mathrm{c}}\} = \{\hat{\theta}_{\kappa+1}, \hat{\theta}_{\kappa+2}, \cdots, \hat{\theta}_\Omega\}$. The symbols on IM and non-IM virtual sub-carriers are elicited as $\hat{\mathcal{X}}_{\mathrm{a}}[k] = \hat{\hat{Y}}[\hat{\theta}_{k+1}]$ for $k \in [\![0, \kappa - 1]\!]$ resulting in $\hat{\boldsymbol{\mathcal{X}}}_{\mathrm{a}} = [\hat{\mathcal{X}}_{\mathrm{a}}[0], \hat{\mathcal{X}}_{\mathrm{a}}[1], \cdots, \hat{\mathcal{X}}_{\mathrm{a}}[\kappa - 1]]^{\mathrm{T}}$ and $\hat{\mathcal{X}}_{\mathrm{b}}[k] = \hat{\hat{Y}}[\hat{\theta}_{k+1}^{\mathrm{c}}]$ for $k \in [\![0, \Omega - \kappa - 1]\!]$ resulting in $\hat{\boldsymbol{\mathcal{X}}}_{\mathrm{b}} = [\hat{\mathcal{X}}_{\mathrm{b}}[0], \hat{\mathcal{X}}_{\mathrm{b}}[1], \cdots, \hat{\mathcal{X}}_{\mathrm{b}}[\Omega - \kappa - 1]]^{\mathrm{T}}$, respectively. Finally, using $\hat{\boldsymbol{\theta}}$, $\hat{\boldsymbol{\mathcal{X}}}_{\mathrm{a}}$ and $\hat{\boldsymbol{\mathcal{X}}}_{\mathrm{b}}$, we attain the bit sequences $\hat{\lambda}_1$, $\hat{\lambda}_2$ and $\hat{\lambda}_3$, respectively.

2) LOW-COMPLEXITY DISJOINT MAXIMUM LIKELIHOOD DETECTOR

To implement the low-complexity disjoint ML detector for EO-OFDM-DM, firstly, the virtual sub-carriers used for IM are determined considering the inner product of $\hat{\hat{\mathbf{Y}}}$ and the constellation alphabet used for IM virtual sub-carriers, $\mathcal{S}_{\mathrm{a}} \in \mathcal{M}_{\mathrm{a}}$ as

$$\alpha[k] = \arg\max_{\mathcal{S}_{\mathrm{a}} \in \mathcal{M}_{\mathrm{a}}} \{\langle \hat{\hat{Y}}[k]; \mathcal{S}_{\mathrm{a}} \rangle\}, \qquad (37)$$

for $k \in [\![0, \Omega - 1]\!]$ which culminates in $\boldsymbol{\alpha} = [\alpha[0], \alpha[1], \cdots, \alpha[\Omega - 1]]^{\mathrm{T}}$. Once we have classified which virtual sub-carriers are likely to modulate alphabets from $\mathcal{M}_{\mathrm{a}}$, then the ML criterion is appraised as in (17), resulting in $\boldsymbol{\gamma}$ which has elements sorted in the ascending order. Subsequently, $\hat{\boldsymbol{\theta}} = \{\hat{\theta}_1, \hat{\theta}_2, \cdots, \hat{\theta}_\Omega\}$ is achieved by adhering to an identical procedure as in EO-OFDM-IM. Thus, the first κ elements of $\boldsymbol{\gamma}$ contain the output of ML criterion for IM virtual sub-carriers, which should be zero under ideal circumstances, while the remaining elements of $\boldsymbol{\gamma}$ indicate the output of ML criterion for non-IM virtual sub-carriers which should be non-zero. Therefore, the SAP at the receiver is determined by retaining the first κ elements of $\hat{\boldsymbol{\theta}} = \{\hat{\theta}_1, \hat{\theta}_2, \cdots, \hat{\theta}_\kappa\}$ and using the remaining to attain $\hat{\boldsymbol{\theta}}^{\mathrm{c}} = \{\hat{\theta}_1^{\mathrm{c}}, \hat{\theta}_2^{\mathrm{c}}, \cdots, \hat{\theta}_{\Omega-\kappa}^{\mathrm{c}}\}$. Lastly, using $\hat{\boldsymbol{\theta}}$, $\hat{\boldsymbol{\theta}}^{\mathrm{c}}$ and $\hat{\hat{\mathbf{Y}}}$, the symbols on IM and non-IM virtual sub-carriers are realized as $\hat{\mathcal{X}}_{\mathrm{a}}[k] = \hat{\hat{Y}}[\hat{\theta}_{k+1}]$ for $k \in [\![0, \kappa - 1]\!]$ and $\hat{\mathcal{X}}_{\mathrm{b}}[k] = \hat{\hat{Y}}[\hat{\theta}_{k+1}^{\mathrm{c}}]$ for $k \in [\![0, \Omega - \kappa - 1]\!]$, respectively. Lastly, $\hat{\lambda}_1$, $\hat{\lambda}_2$ and $\hat{\lambda}_3$ are respectively determined using $\boldsymbol{\theta}$, $\hat{\boldsymbol{\mathcal{X}}}_{\mathrm{a}}$ and $\hat{\boldsymbol{\mathcal{X}}}_{\mathrm{b}}$.

VI. PERFORMANCE ANALYSIS OF EO-OFDM-DM

In this section, we examine the performance of EO-OFDM-DM considering the same criteria we adopted for EO-OFDM-IM. Firstly, we appraise the SE of EO-OFDM-DM schemes and compare it with that of classical O-OFDM-DM approaches. Secondly, we investigate the EE of EO-OFDM-DM schemes and determine the optimal approach among EO-OFDM-IM and EO-OFDM-DM which could be utilized within a given SE region. Lastly, we determine the BER performance of the schemes considering LOS and time dispersive propagation.

A. SPECTRAL EFFICIENCY ANALYSIS

The number of bits, λ transmitted per EO-OFDM-DM symbol of duration $T_{\rm s}$ is given by (35), which results in a data rate of $R = \lambda/T_{\rm s}$. Moreover, the base-band bandwidth needed by EO-OFDM-DM is same as that of EO-OFDM-IM, which is given by (19). Thus, the SE $\eta = R/B$ for EO-OFDM-DM in bits/s/Hz is

$$\eta = \begin{cases} \dfrac{2\left(\left\lfloor \log_2\binom{\Omega}{\kappa}\right\rfloor + \log_2(M_{\rm a}^{\kappa}M_{\rm b}^{\Omega-\kappa})\right)}{\mathcal{N}}, & \text{DCEO-OFDM-DM} \\[4mm] \dfrac{\left\lfloor \log_2\binom{\Omega}{\kappa}\right\rfloor + \log_2(M_{\rm a}^{\kappa}M_{\rm b}^{\Omega-\kappa})}{\mathcal{N}}, & \text{ACEO-OFDM-DM.} \end{cases} \tag{38}$$

The approximate κ required to attain the peak η for EO-OFDM-DM approaches is evaluated in Lemma 2. It may be noticed that Lemma 1 can be generalized using Lemma 2 by considering $M_{\rm b} = 1$.

On the other hand, the number of bits transmitted per O-OFDM-DM symbol of duration $\tilde{T}_{\rm s}$ is

$$\tilde{\lambda} = \left\lfloor \log_2\binom{\tilde{\Omega}}{\tilde{\kappa}}\right\rfloor + \log_2(\tilde{M}_{\rm a}^{\tilde{\kappa}}\tilde{M}_{\rm b}^{\tilde{\Omega}-\tilde{\kappa}}), \tag{39}$$

which affords a data rate of $\tilde{R} = \tilde{\lambda}/\tilde{T}_{\rm s}$. The base-band requirement of O-OFDM-DM is same as that of O-OFDM-IM given in (23). Hence, the SE $\tilde{\eta} = \tilde{R}/\tilde{B}$ of O-OFDM-DM in bits/s/Hz is appraised to be

$$\tilde{\eta} = \begin{cases} \dfrac{2\left(\left\lfloor \log_2\binom{\tilde{\Omega}}{\tilde{\kappa}}\right\rfloor + \log_2(\tilde{M}_{\rm a}^{\tilde{\kappa}}\tilde{M}_{\rm b}^{\tilde{\Omega}-\tilde{\kappa}})\right)}{\mathcal{N}}, & \text{DCO-OFDM-DM} \\[4mm] \dfrac{\left\lfloor \log_2\binom{\tilde{\Omega}}{\tilde{\kappa}}\right\rfloor + \log_2(\tilde{M}_{\rm a}^{\tilde{\kappa}}\tilde{M}_{\rm b}^{\tilde{\Omega}-\tilde{\kappa}})}{\mathcal{N}}, & \text{ACO-OFDM-DM.} \end{cases} \tag{40}$$

Lemma 2: Considering Ω, the peak SE for EO-OFDM-DM schemes employing alphabets $\mathcal{M}_{\rm a}$ of cardinality $M_{\rm a}$ for IM virtual sub-carrier and alphabets $\mathcal{M}_{\rm b}$ of cardinality $M_{\rm b}$ for non-IM virtual sub-carriers is realized if the number of virtual sub-carriers for IM are approximately

$$\kappa_{\rm approx} \approx \left\lfloor \frac{M_{\rm a}\Omega}{M_{\rm a} + M_{\rm b}}\right\rfloor. \tag{41}$$

Proof: The SE of EO-OFDM-DM with parameters $\{\Omega, M_{\rm a}, M_{\rm b}\}$ varies with κ. Moreover, η is maximum when λ is maximum. Thus, considering (35) and ignoring the floor function, one obtains

$$\lambda \leq \log_2\binom{\Omega}{\kappa} + \log_2(M_{\rm a}^{\kappa}M_{\rm b}^{\Omega-\kappa}). \tag{42}$$

Taking the derivative of (42) with respect to κ yields

$$\frac{d\lambda}{d\kappa} \leq \frac{\psi_{\Omega-\kappa} - \psi_{\kappa} + \log(\frac{M_{\rm a}}{M_{\rm b}})}{\log(2)}. \tag{43}$$
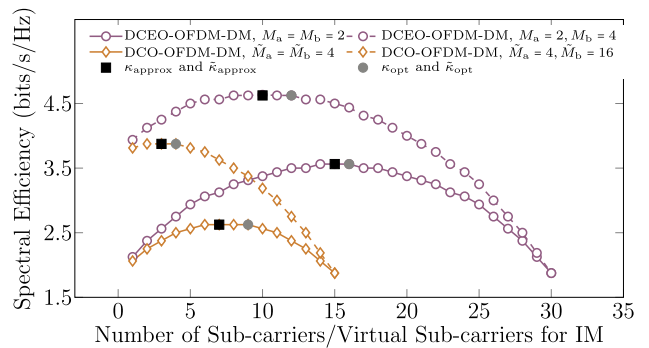

FIGURE 18. SE evolution of DCEO-OFDM-DM and DCO-OFDM-DM with respect of number of active sub-carriers/virtual sub-carriers.

Substituting the approximation of harmonic number in (43) and equating $d\lambda/d\kappa$ equal to zero, we obtain

$$\kappa \leq \frac{M_{\rm a}\Omega}{M_{\rm a} + M_{\rm b}}. \tag{44}$$

By reintroducing the floor function, the approximate value of κ, i.e., $\kappa_{\rm approx}$ is obtained as in (41). ∎

Similarly, for O-OFDM-DM schemes with parameters, $\{\tilde{\Omega}, \tilde{M}_{\rm a}, \tilde{M}_{\rm b}\}$, the approximate number of complex-valued sub-carriers which have to be modulated to realize the peak SE is

$$\tilde{\kappa}_{\rm approx} \approx \left\lfloor \frac{\tilde{M}_{\rm a}\tilde{\Omega}}{\tilde{M}_{\rm a} + \tilde{M}_{\rm b}}\right\rfloor. \tag{45}$$

Note that for EO-OFDM-DM (resp. O-OFDM-DM) schemes, we likewise have an optimal κ, i.e., $\kappa_{\rm opt}$ (resp. $\tilde{\kappa}_{\rm opt}$) which determines the minimum number of virtual sub-carrier (resp. complex-valued sub-carriers) for IM to culminates the peak SE. We accentuate that it is also necessary to keep the virtual sub-carriers for IM in EO-OFDM-DM schemes to the minimal possible value, otherwise, $E_{\rm b(elec)}$ increases which reduces EE.

Fig. 18 illustrates the SE evolution of DCEO-OFDM-DM (resp. DCO-OFDM-DM) schemes by varying κ (resp. $\tilde{\kappa}$) for IM considering $\mathcal{N} = 32$. For DCEO-OFDM-DM, we utilize parameters $\{M_{\rm a}, M_{\rm b}\} = \{2, 2\}$ and $\{M_{\rm a}, M_{\rm b}\} = \{2, 4\}$ culminating in spectral efficiencies of $\eta = \{2.125 \rightarrow 3.5625\}$ bits/s/Hz for $\kappa \in [\![1, 14]\!]$ and $\eta = \{3.9375 \rightarrow 4.625\}$ when $\kappa \in [\![1, 8]\!]$, respectively. The peak SE attained using $\{M_{\rm a}, M_{\rm b}\} = \{2, 2\}$ for DCEO-OFDM-IM is $\eta = 3.5625$ bits/s/Hz which is within 5% of the SE of DCO-OFDM when $\dot{M} = 16$ which is $\dot{\eta} = 3.75$ bits/s/Hz. For DCO-OFDM-DM, we use $\{\tilde{M}_{\rm a}, \tilde{M}_{\rm b}\} = \{4, 4\}$ and $\{\tilde{M}_{\rm a}, \tilde{M}_{\rm b}\} = \{4, 16\}$; which results in SE of $\tilde{\eta} = \{2.0625 \rightarrow 2.625\}$ bits/s/Hz when $\tilde{\kappa} \in [\![1, 6]\!]$ and $\tilde{\eta} = \{3.8125 \rightarrow 3.875\}$ bits/s/Hz and $\tilde{\kappa} \in [\![1, 2]\!]$, respectively. We can recognize that with low alphabet cardinalities, $\tilde{\eta}$ does not come close to the $\dot{\eta}$ with $\dot{M} = 16$ which is 3.75 bits/s/Hz. We observe the following advantages of DCEO-OFDM-DM over counterparts from Fig. 18. First, DCEO-OFDM-DM provides the ability to attain higher spectral efficiencies than the counterparts, e.g., with $\{M_{\rm a}, M_{\rm b}\} = \{2, 2\}$, it yields 57.15% higher peak SE than DCO-OFDM-DM with $\{\tilde{M}_{\rm a}, \tilde{M}_{\rm b}\} = \{4, 4\}$. Secondly, the granularity in
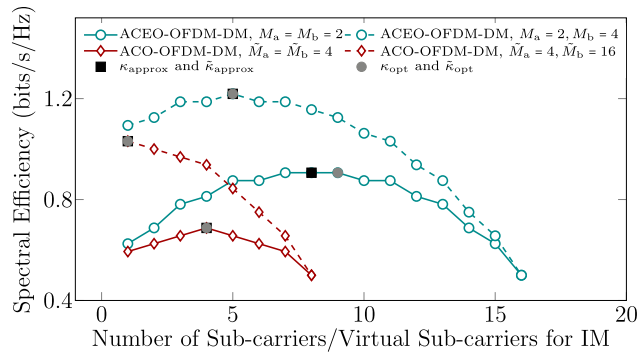
FIGURE 19. SE evolution of ACEO-OFDM-DM and ACO-OFDM-DM with respect of number of active sub-carriers/virtual sub-carriers.

FIGURE 20. The evolution of required $E_{b_{(elec)}}/N_0$ considering optimal approach among DCEO-OFDM-IM, DCO-OFDM-IM, DCEO-OFDM-DM and DCO-OFDM-DM in terms of EE for a given η and $\tilde{\eta}$ for target BER of 10^{-3}. The EE versus SE performance of DCO-OFDM with $\dot{M} \in \{4, 16\}$ is also presented as benchmark.

FIGURE 21. The evolution of required $E_{b_{(elec)}}/N_0$ for ACEO-OFDM-DM, ACO-OFDM-DM and ACO-OFDM-IM for target BER of 10^{-3}.

terms of the number of operating points along the curve for DCEO-OFDM-DM is higher (14 compared to 6) than DCO-OFDM-DM, which reinforces the adaptability of DCEO-OFDM-DM. We can observe that to match the peak SE of DCEO-OFDM-DM when $\{M_a, M_b\} = \{2, 2\}$, DCO-OFDM-DM will have to employ $\{\tilde{M}_a, \tilde{M}_b\} = \{4, 16\}$, which would be detrimental in terms of EE.

Fig. 19 portrays the evolution of SE of ACEO-OFDM-DM by changing the number of virtual sub-carrier for IM and comparing it with that of ACO-OFDM-DM considering $\mathcal{N} = 32$. ACEO-OFDM-IM with $\{M_a, M_b\} = \{2, 2\}$ allows SE of $\eta = \{0.625 \to 0.9063\}$ bits/s/Hz for $k \in [\![1, 7]\!]$, with peak SE within 10% of the SE of ACO-OFDM with $\dot{M} = 16$. ACO-OFDM-DM with $\{\tilde{M}_a, \tilde{M}_b\} = \{4, 4\}$ provides spectral efficiencies between $\tilde{\eta} = \{0.5938 \to 0.6875\}$ bits/s/Hz when $\tilde{\kappa} \in [\![1, 4]\!]$. With the above parameters, the peak SE offered by ACEO-OFDM-DM is approximately 35.46% higher than that of ACO-OFDM-DM. When $\{M_a, M_b\} = \{2, 4\}$, the SE can vary between $\eta = \{1.0938 \to 1.2188\}$ bits/s/Hz for $\kappa \in [\![1, 7]\!]$, whereas, ACO-OFDM-DM can afford only $\tilde{\eta} = 1.0938$ for $\tilde{\kappa} = 1$ when $\{\tilde{M}_a, \tilde{M}_b\} = \{4, 16\}$ with no granularity for EE/SE trade-off. Obviously, in this case, one can change $\tilde{\kappa}$ to realize lower SE and provide granularity but at the cost of EE. For EO-OFDM-DM schemes, the region of interest is for spectral efficiencies obtained using $\{M_a, M_b\} = \{2, 2\}$.

It is highlighted that DCEO-OFDM-DM can be employed for high SE OWS, whereas, ACEO-OFDM-DM can be used for energy-efficient OWS, where a higher SE compared to the peak SE of ACEO-OFDM is needed.

B. ENERGY EFFICIENCY ANALYSIS

In this section, apart from portraying the EE for EO-OFDM-DM approaches, we also provide the optimal setups regarding IM or DM approaches and alphabet cardinalities to target particular SE ranges.

First, we investigate the EE performance of DCEO-OFDM-DM. Fig. 20 presents the EE/SE trade-off of DCEO-OFDM-DM when $\mathcal{N} = 32$. For targeting SE between the range $\eta \in [2.75, 3.5625]$ bits/s/Hz, the optimal scheme is DCEO-OFDM-DM with $\{M_a, M_b\} = \{2, 2\}$.
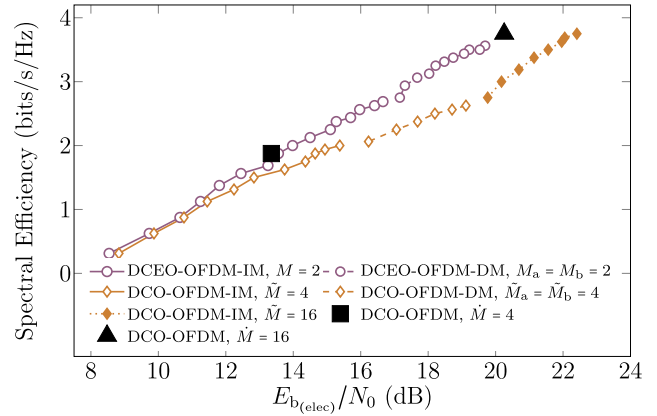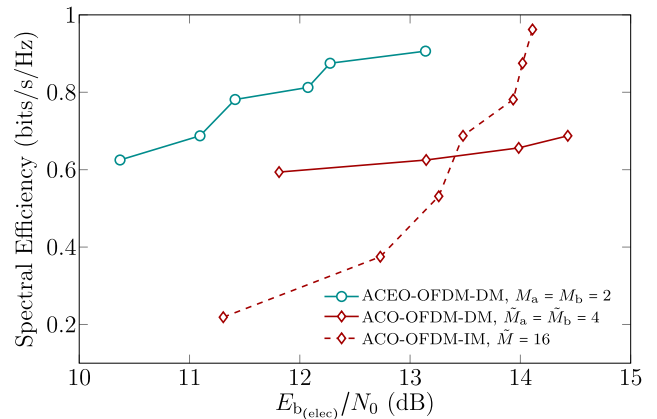
Whereas the spectral efficiencies between the ranges $\eta \in [0.3125, 2.75[$ bits/s/Hz can optimally be obtained utilizing DCEO-OFDM-IM with $M = 2$. As aforementioned, the peak SE of DCEO-OFDM-DM considering $\{M_a, M_b\} = \{2, 2\}$ is within 5% of the SE of DCO-OFDM. Now, if we consider DCO-OFDM-DM, the optimal range of SE which can be targeted when $\{\tilde{M}_a, \tilde{M}_b\} = \{4, 4\}$ is $\tilde{\eta} \in [2.0625, 2.625]$ bits/s/Hz, whereas, to target SE range between $\tilde{\eta} \in [0.3125, 2]$ bits/s/Hz, DCO-OFDM-IM with $\tilde{M} = 4$ is the best choice. Moreover, spectral efficiencies between $\tilde{\eta} \in [2.75, 3.75]$ bits/s/Hz with optimal performance is attained using DCO-OFDM-IM with $\tilde{M} = 16$. From Fig. 20, we observe that both DCEO-OFDM-IM and DCEO-OFDM-DM not only provide better SE but also a better EE, which becomes distinctive for spectral efficiencies > 1 bits/s/Hz. Furthermore, DCEO-OFDM-DM is much more energy-efficient than DCO-OFDM-DM.

Fig. 21 provides the EE/SE trade-off performance of ACEO-OFDM-DM and compares it with that of ACO-OFDM-DM. We consider $\mathcal{N} = 32$ sub-carriers, $\{M_a, M_b\} = \{2, 2\}$ for ACEO-OFDM-DM and $\{\tilde{M}_a, \tilde{M}_b\} = \{4, 4\}$ for
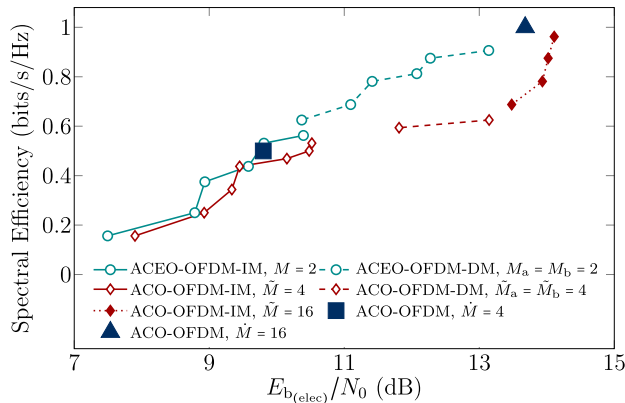
FIGURE 22. The evolution of required $E_{b_{(elec)}}/N_0$ considering optimal approach among ACEO-OFDM-IM, ACO-OFDM-IM, ACEO-OFDM-DM and ACO-OFDM-DM in terms of EE for a given η and $\tilde{\eta}$ for target BER of 10^{-3}. The EE versus SE performance of ACO-OFDM with $\dot{M} \in \{4, 16\}$ is also presented as benchmark.

ACO-OFDM-DM. We also provide the EE performance of ACO-OFDM-IM with $\tilde{M} = 16$ for comparison. With $\{M_a, M_b\} = \{2, 2\}$, the spectral efficiencies between the range $\eta \in [0.625, 0.9063]$ bits/s/Hz is optimally attained with ACEO-OFDM-DM. Furthermore, it can be recognized that ACEO-OFDM-DM with above-mentioned parameters is energy-efficient compared to ACO-OFDM-DM, for which, necessarily two operating points at spectral efficiencies $\tilde{\eta}$ of 0.5938 bits/s/Hz and 0.625 bits/s/Hz are useful in terms of EE/SE trade-off, after which, the performance of ACO-OFDM-IM with $\tilde{M} = 16$ is better for spectral efficiencies between the range $\tilde{\eta} \in [0.6875, 1]$ bits/s/Hz. Thus, for the optimal performance, a combination of ACO-OFDM-DM with $\{\tilde{M}_a, \tilde{M}_b\} = \{4, 4\}$ and ACO-OFDM-IM with $\tilde{M} = 16$ should be used to reach the SE of $\dot{\eta} = 1$ of ACO-OFDM, which is attained using $\dot{M} = 16$.

Fig. 22 presents the EE/SE trade-off of ACEO-OFDM-IM and ACEO-OFDM-DM. It can be noticed that ACEO-OFDM-IM with $M = 2$ can target the spectral efficiencies between $\eta \in [0.1563, 0.5625]$ bits/s/Hz, whilst, for spectral efficiencies between $\eta \in [0.625, 0.9063]$ bits/s/Hz can be optimally attained in terms of EE with ACEO-OFDM-DM using $\{M_a, M_b\} = \{2, 2\}$. The optimal combination of operating ACO-OFDM-IM and ACO-OFDM-DM consists of three parts. For the spectral efficiencies between $\tilde{\eta} \in [0.1563, 0.5313]$ bits/s/Hz, ACO-OFDM-IM with $\tilde{M} = 4$ provides the optimal EE/SE trade-off. Thereafter, for ACO-OFDM-DM with $\{\tilde{M}_a, \tilde{M}_b\} = \{4, 4\}$ is optimal between $\tilde{\eta} \in [0.5938, 0.625]$ bits/s/Hz. For spectral efficiencies between $\tilde{\eta} \in [0.6875, 1]$, ACO-OFDM-IM with $\tilde{M} = 16$ provides better performance. It can be observed that generally ACEO-OFDM-IM and ACEO-OFDM-DM schemes provide better EE/SE performance.

C. BIT ERROR RATE ANALYSIS
Fig. 23 and 24 illustrates the BER performance of EO-OFDM-DM schemes using both energy detector receiver
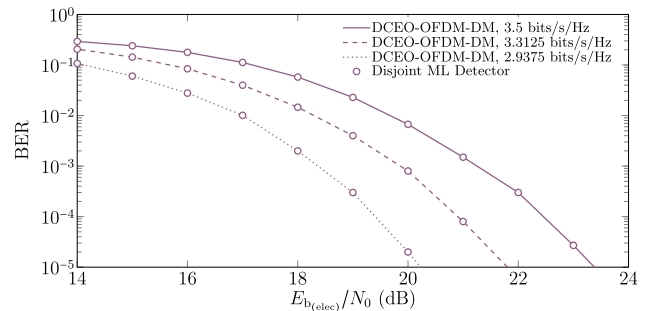

FIGURE 23. BER performance DCEO-OFDM-DM for $\eta = \{2.9375, 3.3125, 3.5\}$ bits/s/Hz for energy detector receiver (lines) and disjoint ML detector receiver (markers).
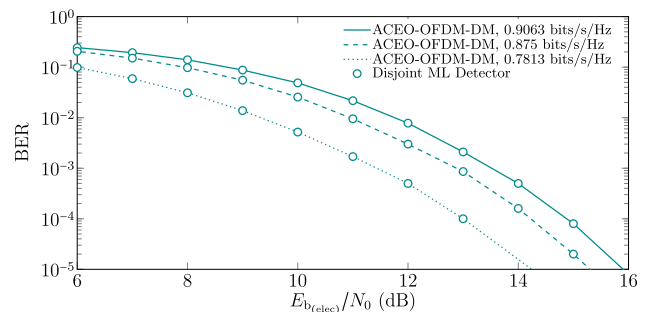

FIGURE 24. BER performance ACEO-OFDM-DM for $\eta = \{0.7813, 0.875, 0.9063\}$ bits/s/Hz for energy detector receiver (lines) and disjoint ML detector receiver (markers).

and disjoint ML receiver for spectral efficiencies which can be targeted within the region of interest. Fig. 23 portrays the BER performance of DCEO-OFDM-DM for $\eta = \{2.9375, 3.3125, 3.5\}$ bits/s/Hz which is realized using $\kappa = \{5, 9, 12\}$ and $\{\mathcal{N}, M_a, M_b\} = \{32, 2, 2\}$. The BER performance of ACEO-OFDM-DM for $\eta = \{0.9063, 0.875, 0.7813\}$ bits/s/Hz is depicted in Fig. 24. These spectral efficiencies are obtained using $\kappa = \{3, 5, 7\}$ and $\{\mathcal{N}, M_a, M_b\} = \{32, 2, 2\}$. These results in Fig. 23 and 24 show that like EO-OFDM-IM schemes, various spectral efficiencies within the region of interest can be targeted with EO-OFDM-DM approaches. Certainly, for DCEO-OFDM-DM and ACEO-OFDM-DM, the region of interest in terms of EE is when the spectral efficiencies are ≥ 2.75 bits/s/Hz and ≥ 0.6875 bits/s/Hz, respectively. Furthermore, we can also notice that the BER performance attained using both detectors is identical.

Next, we investigate the BER performance of EO-OFDM-DM approaches within their region of interest and compare it with that of classical counterparts in both LOS and time dispersive propagation. First, consider Fig. 25 which depicts the BER performance of DCEO-OFDM-DM at $\eta = 3.5$ bits/s/Hz and compare it with that of DCO-OFDM-IM and DCO-OFDM for the same SE. DCO-OFDM-IM with $\tilde{M} = 16$ is used to attain the optimal EE performance for the reference SE (cf. Fig. 20). The SE of 3.5 bits/s/Hz for DCEO-OFDM-DM, DCO-OFDM-IM and DCO-OFDM is attained
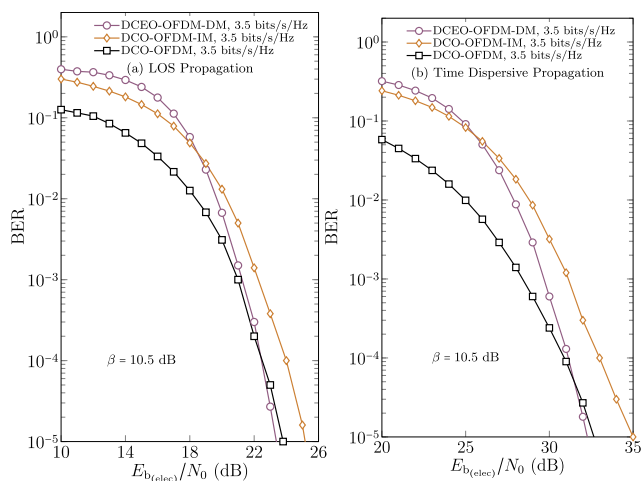
FIGURE 25. BER performance comparison of DCEO-OFDM-DM, DCO-OFDM-IM and DCO-OFDM for a reference SE of 3.5 bits/s/Hz considering. (a) LOS propagation; and (b) time dispersive propagation.
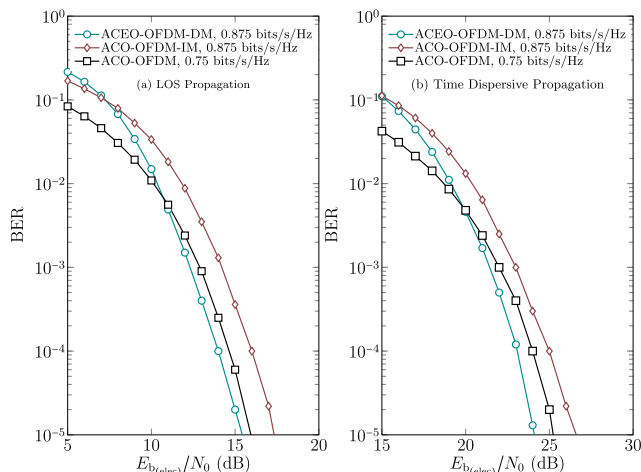

FIGURE 26. BER performance comparison of ACEO-OFDM-IM, ACO-OFDM-IM and ACO-OFDM for a reference SE of 0.875 bits/s/Hz considering. (a) LOS propagation; and (b) time dispersive propagation.

considering $\{\mathcal{N}, M_a, M_b, \kappa\} = \{32, 2, 2, 12\}$, $\{\mathcal{N}, \tilde{M}, \tilde{\kappa}\} = \{32, 16, 12\}$ and $\{\mathcal{N}, \dot{M}\} = \{16, 16\}$, respectively. For a fair comparison, a bias of 10.5 dB is used for all approaches. It can be observed that the DCEO-OFDM-DM affords virtually the same performance as that of DCO-OFDM for higher values of $E_{b_{(elec)}}/N_0$ in both LOS and time dispersive propagation. The added advantage of DCEO-OFDM-DM is its effectiveness to attain different operating points on the EE/SE curve (cf. Fig. 20). It is affirmed that the SE of 3.5625 bits/s/Hz can also be obtained using DCEO-OFDM-IM with parameters $\{\mathcal{N}, M, \kappa\} = \{32, 4, 15\}$. Nonetheless, as aforementioned, DCEO-OFDM-IM loses its EE for $M = 4$, hence, it is better to adopt DCEO-OFDM-DM with above-mentioned parameters. Moreover, we observe that DCO-OFDM-IM is the least energy-efficient approach among the ones considered here.

Fig. 26 compares the BER performance of ACEO-OFDM-DM with ACO-OFDM-IM and ACO-OFDM for a reference SE of 0.875 bits/s/Hz. The reference SE for ACEO-OFDM-DM and ACO-OFDM-IM is attained using $\{\mathcal{N}, M_a, M_b, \kappa\} = \{16, 2, 2, 10\}$ and $\{\mathcal{N}, \tilde{M}, \tilde{\kappa}\} = \{32, 16, 6\}$. Note we have established in Fig. 22 that for 0.875 bits/s/Hz, ACO-OFDM-IM is more energy-efficient than ACO-OFDM-DM. Because of limited granularity of ACO-OFDM, the closest SE that can be realized is 0.75 bits/s/Hz using $\{\mathcal{N}, \dot{M}\} = \{32, 8\}$. It can be observed that ACEO-OFDM-DM is the most energy-efficient approach among all at the given SE. The BER of ACO-OFDM is higher than that of ACEO-OFDM-DM even at a lower SE of (0.75 bits/s/Hz in comparison to 0.875 bits/s/Hz for ACEO-OFDM-DM). Now if we compare the performance of ACEO-OFDM-DM relative to ACO-OFDM-IM, we can observe that for a similar SE, the BER of ACEO-OFDM-DM is much better than ACO-OFDM-IM. These results indicate the ACEO-OFDM-DM is more energy-efficient compared to the alternative schemes.

The results in this section indicate that EO-OFDM-DM approaches can be effectively used for OWS compared to the state-of-the art. Obviously, DCEO-OFDM-DM can be used for high spectral efficiencies and ACEO-OFDM-DM where low spectral efficiencies with high EE is needed.

VII. CONCLUSIONS

In this work, we propose EO-OFDM-IM and EO-OFDM-DM approaches for ItM-DD based OWS. The foremost advantage of these approaches is their effectiveness to obtain higher spectral efficiencies compared to classical counterparts by using so-called virtual sub-carriers. Additionally, these approaches yield comprehensive granularity to target different energy efficiencies and/or spectral efficiencies, while this feature is impossible for classical O-OFDM approaches. Using the proposed approaches, we can target a wide range of applications with wide range of requirements, e.g., energy-efficient IoT based on OWS and high data rate indoor optical wireless communications. We have shown that EO-OFDM-IM schemes always provide better SE/EE performance compared to O-OFDM-IM and O-OFDM counterparts. On the other hand, EO-OFDM-DM approaches manifest at least the same EE as that of O-OFDM counterparts for high $E_{b_{(elec)}}/N_0$, while providing a comprehensive EE/SE trade-off capability. All the results demonstrate that EO-OFDM-IM approaches are the superior choices for IoT and mid-to-high data rate OWS. On the other hand, EO-OFDM-DM approaches can be used for high data rate systems having the same EE as that of O-OFDM with the added advantage of granularity in EE/SE trade-off. Furthermore, we have introduced two low-complexity detectors with identical performances for the proposed approaches. Also, this is the first study which uses the efficient PT based index mapping and de-mapping for IM based approaches. All the advantages of the proposed approaches presented hereby make them up to par

candidates for OWS which can target both low and high spectral efficiencies.

REFERENCES

[1] S. D. Dissanayake and J. Armstrong, "Comparison of ACO-OFDM, DCO-OFDM and ADO-OFDM in IM/DD systems," *J. Lightw. Technol.*, vol. 31, no. 7, pp. 1063–1072, Apr. 2013.

[2] J. Armstrong and B. Schmidt, "Comparison of asymmetrically clipped optical OFDM and DC-biased optical OFDM in AWGN," *IEEE Commun. Lett.*, vol. 12, no. 5, pp. 343–345, May 2008.

[3] S. Mazahir, A. Chaaban, H. Elgala, and M.-S. Alouini, "Achievable rates of multi-carrier modulation schemes for bandlimited IM/DD systems," *IEEE Trans. Wireless Commun.*, vol. 18, no. 3, pp. 1957–1973, Mar. 2019.

[4] D. Tsonev, S. Sinanovic, and H. Haas, "Novel unipolar orthogonal frequency division multiplexing (U-OFDM) for optical wireless," in *Proc. IEEE 75th Veh. Technol. Conf. (VTC Spring)*, May 2012, pp. 1–5.

[5] Q. Wang, C. Qian, X. Guo, Z. Wang, D. G. Cunningham, and I. H. White, "Layered ACO-OFDM for intensity-modulated direct-detection optical wireless transmission," *Opt. Express*, vol. 23, no. 9, pp. 12382–12393, May 2015.

[6] A. W. Azim, Y. Le Guennec, and G. Maury, "Spectrally augmented hartley transform precoded asymmetrically clipped optical OFDM for VLC," *IEEE Photon. Technol. Lett.*, vol. 30, no. 23, pp. 2029–2032, Dec. 1, 2018.

[7] D. Tsonev, S. Videv, and H. Haas, "Unlocking spectral efficiency in intensity modulation and direct detection systems," *IEEE J. Sel. Areas Commun.*, vol. 33, no. 9, pp. 1758–1770, Sep. 2015.

[8] E. Basar, M. Wen, R. Mesleh, M. Di Renzo, Y. Xiao, and H. Haas, "Index modulation techniques for next-generation wireless networks," *IEEE Access*, vol. 5, pp. 16693–16746, 2017.

[9] T. Mao, Q. Wang, Z. Wang, and S. Chen, "Novel index modulation techniques: A survey," *IEEE Commun. Surveys Tuts.*, vol. 21, no. 1, pp. 315–348, 1st Quart., 2019.

[10] E. Başar and E. Panayırcı, "Optical OFDM with index modulation for visible light communications," in *Proc. 4th Int. Workshop Opt. Wireless Commun. (IWOW)*, Sep. 2015, pp. 11–15.

[11] Q. Wang, T. Mao, Z. Wang, and J. Y. Wang, "Index modulation-aided OFDM for visible light communications," in *Visible Light Communications*. Rijeka, Croatia: InTech, 2017.

[12] A. W. Azim, M. Chafii, Y. Le Guennec, and L. Ros, "Spectral and energy efficient fast-OFDM with index modulation for optical wireless systems," *IEEE Commun. Lett.*, early access, Apr. 22, 2020, doi: 10.1109/LCOMM. 2020.2989633.

[13] A. W. Azim, A. Rullier, Y. Le Guennec, L. Ros, and G. Maury, "Energy efficient M-ary frequency-shift keying-based modulation techniques for visible light communication," *IEEE Trans. Cogn. Commun. Netw.*, vol. 5, no. 4, pp. 1244–1256, Dec. 2019.

[14] T. Mao, R. Jiang, and R. Bai, "Optical dual-mode index modulation aided OFDM for visible light communications," *Opt. Commun.*, vol. 391, pp. 37–41, May 2017.

[15] M. Irfan and S. Aïssa, "On the spectral efficiency of orthogonal frequency-division multiplexing with index modulation," in *Proc. IEEE Global Commun. Conf. (GLOBECOM)*, Dec. 2018, pp. 1–6.

[16] E. Başar, U. Aygölü, E. Panayırcı, and V. Poor, "Orthogonal frequency division multiplexing with index modulation," *IEEE Trans. Signal Process.*, vol. 61, no. 22, pp. 5536–5549, Nov. 2013.

[17] S. Queiroz, J. P. Vilela, and E. Monteiro, "Optimal mapper for OFDM with index modulation: A spectro-computational analysis," *IEEE Access*, vol. 8, pp. 68365–68378, 2020.

[18] S. Queiroz, J. Vilela, and E. Monteiro, "What is the cost of the index selector task for OFDM with index modulation?" in *Proc. Wireless Days*, Apr. 2019, pp. 1–8.

[19] A. W. Azim, Y. Le Guennec, and L. Ros, "Hybrid frequency and phase-shift keying modulation for energy efficient optical wireless systems," *IEEE Wireless Commun. Lett.*, vol. 9, no. 4, pp. 429–432, Apr. 2020.

[20] S. Queiroz, W. Silva, J. P. Vilela, and E. Monteiro, "Maximal spectral efficiency of OFDM with index modulation under polynomial space complexity," *IEEE Wireless Commun. Lett.*, vol. 9, no. 5, pp. 679–682, May 2020.

[21] P. K. Frenger and N. A. B. Svensson, "Parallel combinatory OFDM signaling," *IEEE Trans. Commun.*, vol. 47, no. 4, pp. 558–567, Apr. 1999.

[22] J. B. Carruthers and J. M. Kahn, "Modeling of nondirected wireless infrared channels," *IEEE Trans. Commun.*, vol. 45, no. 10, pp. 1260–1268, Oct. 1997.

ALI WAQAR AZIM received the bachelor's degree in electrical engineering from the COMSATS Institute of Information Technology (CIIT), Islamabad, Pakistan, in 2011, the Diplôme d'ingénieur from ENSIMAG, Grenoble-INP, the master's degree in electronic engineering from the Politecnico di Torino, Italy, and the Ph.D. degree in optics and radio-frequency from Université Grenoble Alpes, in 2018. He worked as a Research Engineer with the GIPSA-Laboratory, Université Grenoble Alpes (UGA) till December 2019. He is currently as an Independent Researcher. His research interests include in the application of signal processing for wireless systems and the design and analysis of modulation schemes for optical wireless communications. He is also serving on the Editorial Board of *Frontiers in Communications and Networks*.

YANNIS LE GUENNEC received the Engineer degree and the Ph.D. degree in optics optoelectronics and microwaves from Grenoble INP, France, in 2000 and 2003, respectively. He is currently an Associate Professor with the GIPSA-Lab, Grenoble, France. His research interests are about visible light communications, wireless communications, optical interconnects, microwave photonics, and all-optical signal processing.

MARWA CHAFII received the master's degree in advanced wireless communication systems (SAR) and the Ph.D. degree in telecommunications from CentraleSupélec, France, in 2013 and 2016, respectively. From 2014 to 2016, she has been a Visiting Researcher with the Poznan University of Technology, Poland, the University of York, U.K., Yokohama National University, Japan, and the University of Oxford, U.K. In February 2018, she joined the Vodafone Chair Mobile Communication Systems at the Technical University of Dresden, Germany, as a Research Group Leader. Since September 2018, she has been a Research Projects Lead with Women in AI and an Associate Professor with ENSEA, France, where she also holds the Chair of Excellence from Paris Seine Initiative. She received the 2018 Ph.D. Prize in the field of signal, image, and vision, in France. She has been listed under the top ten Rising Stars at N2Women. Her research interests include signal processing for digital communications, advanced waveform design for wireless communications, and machine learning for communications. She currently serves as an Associate Editor for the IEEE COMMUNICATIONS LETTERS. She is the Vice-Chair of the IEEE ComSoc Emerging Technology Initiative on Machine Learning for Communications. She is also currently managing the Gender Committee of the AI4EU community.

LAURENT ROS received the degree in electrical engineering from Supelec, Paris, France, in 1992, and the Ph.D. and H.D.R. (accreditation to supervise research) degrees in signal processing and telecoms from the University of Grenoble, in 2001 and 2016, respectively. From 1993 to 1995, he worked on transmission for submarine applications with France-Telecom Research and Development, Lannion. From 1995 to 1999, he worked as a Research and Development Project Leader with Sodielec, Millau, on the design of digital modems and audio codecs for telecoms equipments. Since 2002, he has been an Associate Professor with Gipsa-Laboratory (ex "the Laboratory-of Image-and-Signal") and the Grenoble-INP Institute of Engineering. His research interest includes signal processing for wireless communications.

● ● ●